

SERI/TR-252-2015  
DE84000080

November 1983

# Air/Molten Salt Direct-Contact Heat-Transfer Experiment and Economic Analysis

Mark S. Bohn



# SERI

## **Solar Energy Research Institute**

A Division of Midwest Research Institute

1617 Cole Boulevard  
Golden, Colorado 80401

Operated for the

**U.S. Department of Energy**

under Contract No. DE-AC02-83CH10093

Solar Energy Research Institute  
1617 Cole Boulevard  
Golden, Colorado 80401

A Division of Midwest Research Institute



**Mark Bohn**  
Senior Research Engineer  
Solar Thermal Research Branch  
(303) 231-1755  
FTS 327-1755

Printed in the United States of America  
Available from:  
National Technical Information Service  
U.S. Department of Commerce  
5285 Port Royal Road  
Springfield, VA 22161

Price:  
Microfiche A01  
Printed Copy A04

#### NOTICE

This report was prepared as an account of work sponsored by the United States Government. Neither the United States nor the United States Department of Energy, nor any of their employees, nor any of their contractors, subcontractors, or their employees, makes any warranty, express or implied, or assumes any legal liability or responsibility for the accuracy, completeness or usefulness of any information, apparatus, product or process disclosed, or represents that its use would not infringe privately owned rights.

**SERI/TR-252-2015**  
**UC Category: 59c**  
**DE8400080**

# **Air/Molten Salt Direct-Contact Heat-Transfer Experiment and Economic Analysis**

**Mark S. Bohn**

**November 1983**

**Prepared under Task No. 4250.00**  
**WPA No. 431-83**

---

## **Solar Energy Research Institute**

A Division of Midwest Research Institute

1617 Cole Boulevard  
Golden, Colorado 80401

Prepared for the  
**U.S. Department of Energy**  
Contract No. DE-AC02-83CH10093

## PREFACE

This report describes a technical and economic evaluation of direct-contact heat transfer for solar energy storage applications. The research involved measuring direct-contact heat-transfer coefficients for an air and molten salt system in a pilot-scale experimental facility, calculating the heat transfer based on mass-transfer data, and comparing the value of direct contact with conventional heat exchanger technology.

I would like to acknowledge the contributions of Robert Barlow, Jack Hill, Raymond Kemna, Kenneth May, and Curtis Stern to the design, construction, and operation of the experiment and the valuable discussions on the economic calculations with Robert Copeland and R. Gerald Nix. I also appreciate the careful technical reviews of this report by Robert Boehm, University of Utah, Robert McMordie, Martin Marietta, and William Thayer, Mathematical Sciences Northwest.



---

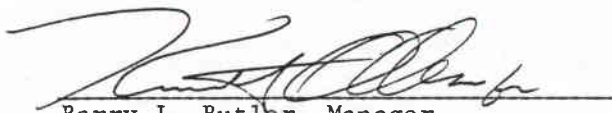
Mark S. Bohn

Approved for

SOLAR ENERGY RESEARCH INSTITUTE



Frank Kreith, Chief  
Thermal Research Branch



Barry L. Butler, Manager  
Solar Thermal and Materials Research Division

## SUMMARY

### Objective

To determine if direct-contact heat exchange is a cost-effective means of transferring heat between air and molten salt.

### Discussion

Direct-contact heat exchange can be used to heat air with molten salt where the salt is used as a heat-transfer fluid in a solar central receiver or as a thermal storage medium. Examples are high-temperature process heat and Brayton power cycles. Prior to this work, heat exchanger data were not available that would allow one to accurately assess the economic value of the direct-contact technique. Analytical methods were available for predicting heat transfer in direct-contact systems; however, as this report shows, those methods are suspect and could lead to significant errors. We measured direct-contact heat-transfer coefficients in a pilot-scale, direct-contact heat exchanger that used a packed column. These heat-transfer data were then used in an economic analysis that compared the direct-contact heat exchanger with a conventional, finned-tube heat exchanger.

### Conclusions

Direct-contact heat exchange provides very high rates of heat transfer per unit volume because of the intimate contact between the air and salt. This enables one to use smaller and, therefore, less costly heat exchangers. In addition, a metal tube wall is not required to separate the two phases. Thus, material requirements are much less stringent since the direct-contact heat exchanger is designed much as a containment vessel. This is especially important for high-temperature applications in which conventional finned-tube heat exchangers require exotic metal alloys. These two advantages make direct-contact heat exchange almost twice as cost-effective as finned-tube exchanges at temperatures up to 600°C. The cost advantage is about fivefold for temperatures from 600°C to 800°C.

TABLE OF CONTENTS

	<u>Page</u>
Nomenclature.....	xi
1.0 Introduction.....	1
2.0 The Heat-Transfer/Mass-Transfer Analogy.....	7
3.0 Experimental Measurements of Volumetric Heat-Transfer Coefficients....	11
3.1 Purpose.....	11
3.2 Description of the Apparatus.....	11
3.3 Instrumentation.....	13
3.4 Column Sizing.....	15
3.5 Operational Problems.....	17
3.6 Heat-Transfer Measurements and Procedures.....	19
3.7 Results and Discussion.....	21
4.0 Economic Analysis.....	25
4.1 Purpose.....	25
4.2 Method of Analysis.....	25
4.3 Materials.....	29
4.4 Effect of Packing Size and Type.....	30
4.5 Results.....	34
5.0 Conclusions and Future Research.....	39
6.0 References.....	41
Appendix A Property Values.....	A-1
Appendix B Cost Methodology for SERI's Solar Energy Storage Program.....	B-1

## LIST OF FIGURES

	<u>Page</u>
1-1 Conventional Finned-Tube Heat Exchanger.....	1
1-2 Direct-Contact Heat Exchanger.....	2
1-3 Three Types of Packing for a Direct-Contact Heat Exchanger.....	3
1-4 Applications of Direct-Contact Heat Exchangers.....	5
2-1 Overall Volumetric Heat-Transfer Coefficients Based on Mass-Transfer Data.....	10
3-1 Flow Diagram of DCHX Test Loop.....	12
3-2 Details of the DCHX Packed Column.....	12
3-3 Photograph of the DCHX Test Apparatus.....	13
3-4 Generalized Pressure Drop Correlation.....	16
3-5 Pressure Drop for Experimental Apparatus.....	16
3-6 Overall Volumetric Heat-Transfer Coefficients Based on Experimental Data.....	21
3-7 Comparison of Measured Heat-Transfer Coefficients for Pall Rings and Raschig Rings.....	23
3-8 Overall System Pressure Drop.....	24
4-1 Layout of the Finned-Tube Heat Exchanger Core.....	28
4-2 Mass-Transfer Coefficient for Various Sizes of Raschig Rings.....	32
4-3 Mass-Transfer Coefficient for Various Types of Packing.....	33
4-4 Cost Comparison for 360°C, 1 atm, 1 MW <sub>th</sub> .....	35
4-5 Cost Comparison for 360°C, 5 atm, 5 MW <sub>th</sub> .....	35
4-6 Cost Comparison for 560°C, 1 atm, 1 MW <sub>th</sub> .....	36
4-7 Cost Comparison for 560°C, 5 atm, 5 MW <sub>th</sub> .....	36
4-8 Cost Comparison for 760°C, 1 atm, 1 MW <sub>th</sub> .....	37
4-9 Cost Comparison for 760°C, 5 atm, 2 MW <sub>th</sub> .....	37

## LIST OF TABLES

	<u>Page</u>
2-1 Parameters for Packed-Column Heat and Mass Transfer.....	9
3-1 Nominal Column Operating Conditions.....	15
3-2 Analysis of Upper Tank Residue.....	18
3-3 Measured Data Showing Effect on $Q_a$ and $U_a$ .....	20
3-4 Heat-Transfer Data and Comparison with Mass-Transfer Calculations.....	22
4-1 Materials of Construction.....	31
4-2 Installed Materials Cost, 760°C DCHX.....	31
4-3 Cost Ratios of Transferring Heat via DCHX Relative to Finned-Tube Heat Exchanger.....	38



## NOMENCLATURE

a	interfacial surface area per unit volume, $m^{-1}$ ( $ft^{-1}$ )
$A_a$	finned-tube heat exchanger surface area, $m^2$ ( $ft^2$ )
AC	levelized annual cost, \$/yr
C	specific heat, $J/kg$ $^{\circ}C$ ( $Btu/lbm$ $^{\circ}F$ )
$C_f$	parameter in $H_d$ correlation
$C_f$	plant capacity factor
$C_p$	specific heat at constant pressure, $J/kg$ $^{\circ}C$ ( $Btu/lbm$ $^{\circ}F$ ); $2.394 \times 10^{-4}$
CI	capital cost, \$
D	mass diffusivity, $m^2/h$ ( $ft^2/h$ ); 10.76
$d_p$	packing size, cm (in.)
$d_t$	column diameter, m (ft)
$f_1$	viscosity function
$f_2$	density function
$f_3$	surface tension function
G	gas-flow rate per unit bed area, $kg/h$ $m^2$ ( $lbm/h$ $ft^2$ ); 0.2044
H	column height or finned-tube exchanger height, m (ft)
$H_d$	height of a transfer unit, m (ft)
h	heat-transfer coefficient, $W/m^2$ $^{\circ}C$ ( $Btu/h$ $ft^2$ $^{\circ}F$ ); 0.1761
k	thermal conductivity, $W/m$ $^{\circ}C$ ( $Btu/h$ $ft$ $^{\circ}F$ ); 0.5777
$k_g$	gas side mass-transfer coefficient, $kg$ $mol/h$ $m^2$ $atm$ ( $lb$ $mol/h$ $ft^2$ $atm$ ); 0.2044
L	liquid flow rate per unit bed area, $kg/h$ $m^2$ ( $lbm/h$ $ft^2$ ); 0.2044
L	length of finned-tube heat exchanger in flow direction, m (ft)
$\dot{m}$	mass flow rate, $kg/h$ ( $lbm/h$ )
m,n	exponents in $H_d$ correlation
OM	operating cost, \$/yr
P	total pressure, atm
$P_{BM}$	logarithmic mean partial pressure of component B, atm
Pr	Prandtl number
Q	heat transfer or heat duty, W ( $Btu/h$ ); 3.412
R	universal gas constant, $m^3$ $atm/^{\circ}C$ $kg$ $mol$ ( $ft^3$ $atm/^{\circ}R$ $lb$ $mol$ ); 8.918
Sc	Schmidt number
T	absolute temperature, $^{\circ}C$ ( $^{\circ}R$ )
$U_a$	overall volumetric heat-transfer coefficient, $W/m^3$ $^{\circ}C$ ( $Btu/h$ $ft^3$ $^{\circ}F$ ); 0.05368

## NOMENCLATURE (Concluded)

V flow velocity, m/h (ft/h)  
 $V_p$  volume of packing bed,  $m^3$  ( $ft^3$ )  
W finned-tube heat exchanger width, m (ft)

## GREEK

$\alpha$  heat-transfer area per volume,  $m^{-1}$  ( $ft^{-1}$ )  
 $\Delta p$  heat exchanger pressure drop,  $N/m^2$  (psi);  $1.451 \times 10^{-4}$   
 $\Delta T_m$  log mean temperature difference,  $^{\circ}C$  ( $^{\circ}F$ )  
 $\mu$  absolute viscosity,  $N\ h/m^2$  (lbm/ft h);  $8.690 \times 10^6$   
 $\nu$  kinematic viscosity,  $m^2/s$  ( $ft^2/s$ ); 10.76  
 $\rho$  density,  $kg/m^3$  (lbm/ft<sup>3</sup>); 0.0623  
 $\sigma$  surface tension, dyne/cm  
 $\phi, \psi$  parameters in  $H_d$  correlation

## SUBSCRIPTS

a air  
g gas  
i inlet  
o outlet  
s salt  
l liquid

## NOTE ON SYSTEM OF UNITS

Since a majority of the chemical engineering literature, especially product literature, continues to use the English system of units, we have not attempted to convert such information into the SI system of units. Any data generated in this study, however, is presented in the SI system. To facilitate conversion between the two systems, the factor for converting SI units to English units follows the more important quantities in the preceding list. For example,  $Ua = 1000\ W/m^3\ ^{\circ}C = 53.68\ Btu/h\ ft^3\ ^{\circ}F$  for a volumetric heat-transfer coefficient.

## SECTION 1.0

## INTRODUCTION

Direct-contact heat transfer is the transfer of heat across the phase boundary of two immiscible fluids, either two liquids or a liquid and a gas. Conventional heat exchange technology involves heat transfer across a solid boundary such as the wall of a steel tube in a shell-and-tube exchanger or across a plate in plate heat exchangers. Where the two fluids do not react and can be separated after the heat exchange has been effected, direct-contact heat exchange (DCHX) has several advantages over conventional heat exchangers: (1) without the intervening wall, a lower thermal resistance is present, and there is no heat exchange surface to foul; (2) intimate mixing of the two fluid streams can produce very high rates of heat transfer; and (3) the heat exchanger design can be simpler, require fewer materials of construction, and allow more flexibility in choice of materials.

*DCHX  
lower  
maint.*

Figure 1-1 depicts a conventional finned-tube heat exchanger, and Figure 1-2 shows a DCHX with a packed column. In the finned-tube heat exchanger one fluid is pumped through the tubes, and the other fluid is pumped over the outside of the tubes. The entire tube bundle is enclosed in the shell, which contains the latter fluid. Sufficient heat-transfer area is provided so, given the temperature differential between the fluids and the heat-transfer

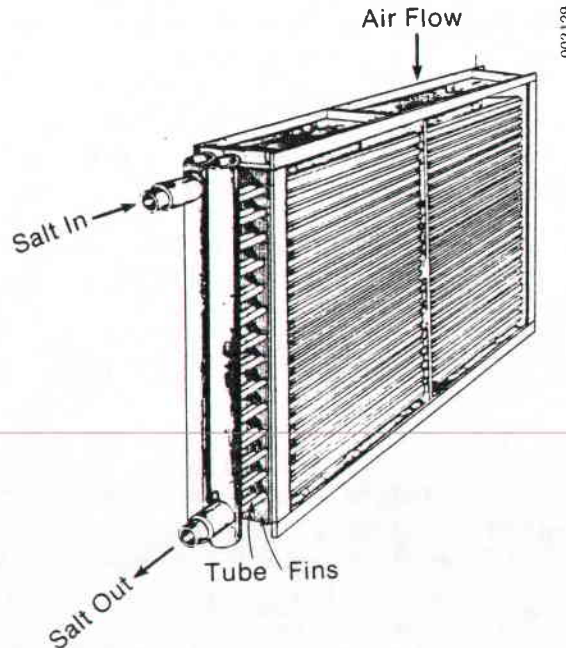


Figure 1-1. Conventional Finned-Tube Heat Exchanger

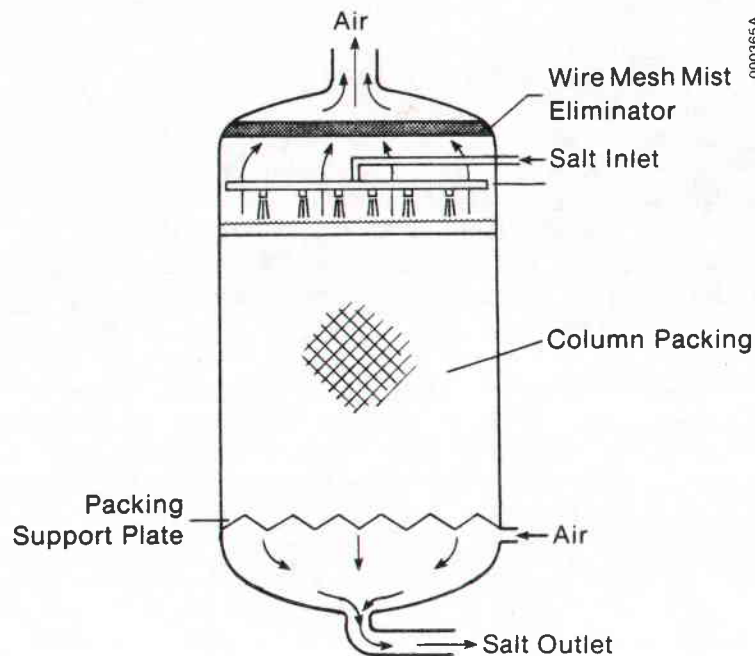


Figure 1-2. Direct-Contact Heat Exchanger

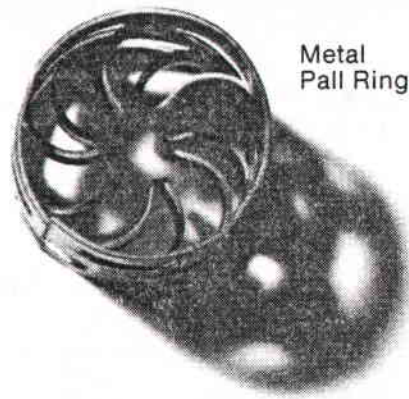
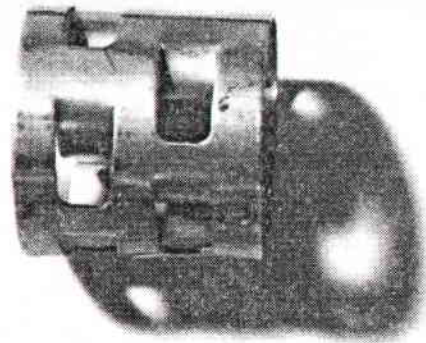
coefficients, the required heat duty can be met. If one or both of the fluids is a gas, it is common to provide fins on the gas side to increase the heat-transfer surface because of the poor heat-transfer characteristics of gases.

The DCHX is a column substantially filled with a packing material. The packing material consists of rings or saddles (Figure 1-3) that are generally 2-3 in. in size for large columns and are dumped in the column in a random arrangement. As shown in Figure 1-2, one fluid enters the top of the vessel and flows downward; the other fluid enters at the bottom of the vessel and flows countercurrent up through the vessel. It is also possible to have a crossflow configuration.

When the DCHX uses a gas and a liquid, the liquid flows downward by gravity and the gas flows upward in the countercurrent configuration. By properly distributing the liquid at the top of the packing, the liquid forms many small rivulets that flow over the packing. These rivulets give a large surface area between the two phases and increase the time during which the liquid stream is exposed to the gas, greatly increasing the rate of heat transfer per unit volume of heat exchanger. We can eliminate the packing by simply spraying the liquid downward and having the gas flow upward in an empty column (i.e., a spray column). Although we did not study the spray column, results of the economic analysis (Section 4.0) indicate that it could offer some advantages over the packed bed at very high temperatures and, therefore, it warrants further investigation.

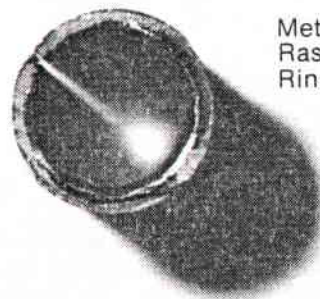
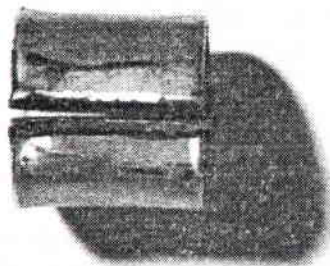
Applications in which DCHX is especially attractive include those in which it is necessary to transfer heat between a gas and a liquid because large heat transfer rates can be achieved without the added expense of finned tubes. In solar thermal technology, two examples include high-temperature process air

*did not study case without packing*

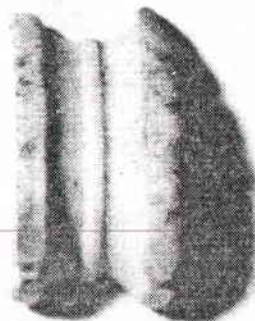


Metal  
Pall Ring

003126



Metal  
Raschig  
Ring



Ceramic  
Intalox  
Saddle

Figure 1-3. Three Types of Packing for a Direct-Contact Heat Exchanger

and the Brayton cycle (shown in Figure 1-4). In both examples, solar energy provides a heat source at a central receiver in which molten salt cools the receiver and transfers the solar energy to a storage device. Molten salt is the logical heat-transfer fluid at high temperatures because it exhibits very low vapor pressure, has high sensible heat storage, has excellent heat-transfer characteristics, and is relatively benign in relation to the receiver containment materials (at temperatures below 600°C for state-of-the-art nitrate salts).

There are two configurations for storing the energy in the molten salt to accommodate the diurnal variation in energy supply or variations in the load. In the first configuration, the molten salt is stored in an insulated vessel providing storage by the sensible heat in the salt. In the second, the salt is used to heat air, which in turn heats a rock bed to provide sensible heat storage. The first method will be necessary for very high temperature applications in which the only material that can tolerate the temperature cycling in the storage is the salt itself. The second storage method is attractive for lower temperature applications (<600°C) because it provides economical, long-term storage. In either storage concept it is necessary to transfer heat from the molten salt to air.

\* Using packed columns is very common in the chemical process industry for mass-transfer operations. One example is the removal of carbon dioxide from a gas stream by contacting the gas stream with monoethanolamine (an organic liquid) or with a hot carbonate solution. The gas is blown up through the bottom of the column, and the monoethanolamine or carbonate solution enters through the top of the column and is distributed over the packing. As a result of this common application and other similar applications, numerous data and design correlations are available for mass-transfer applications, but very little of this information is available for heat-transfer applications.

Because of this lack of heat-transfer data or design correlations, we cannot accurately assess the economic potential of direct-contact heat exchange. Such an assessment requires one to determine the rate of heat transfer per unit volume in the DCHX. This determines the required size and cost of the column to deliver the required amount of heat to the air. It also helps one in determining the costs associated with operating the equipment, primarily the cost of blowing the air through the column.

It is possible to use mass-transfer data by invoking the mass-transfer/heat-transfer analogy (Fair 1972). However, there are several reasons to suspect this approach. Some mechanisms of heat transfer have no analogy to mass transfer. Fair's mass-transfer data and correlations are generally for experiments on water/carbon dioxide systems or water/sodium hydroxide systems. The wetting of the packing by the molten salt probably differs from that of water, and this affects how much interfacial surface area is created by the flow down the packing. Heat may be transferred by conduction in the packing, thereby transferring heat from the dry parts of the packing to the air. This fin effect has no analogy in mass transfer. At high temperatures, radiation heat transfer may be significant, and this mechanism also has no mass-transfer analogy. One may conclude that the calculations of heat transfer based on the mass-transfer analogy as given in Fair (1972) may underestimate the heat-transfer coefficients.

SANDIA LABORATORIES ROUTING SLIP

SF 1888-A(10-77)

R O U T I N G  S E Q U E N C E	ORG.	BLDG.	NAME	COMMENTS OF RECIPIENT								
	6226		<del>W. HOLMES</del>									
	6226		G. KOLB									
	6226		C. TYNER									
			HOLMES									
FROM	J. HOLMES			<table border="1"> <tr> <td>ORG.</td> <td>BLDG.</td> <td>PHONE</td> <td>DATE</td> </tr> <tr> <td>6226</td> <td></td> <td>4-6871</td> <td>6/19</td> </tr> </table>	ORG.	BLDG.	PHONE	DATE	6226		4-6871	6/19
ORG.	BLDG.	PHONE	DATE									
6226		4-6871	6/19									

SENDER'S REMARKS \_\_\_\_\_

\_\_\_\_\_

\_\_\_\_\_

\_\_\_\_\_

\_\_\_\_\_

\_\_\_\_\_

003130

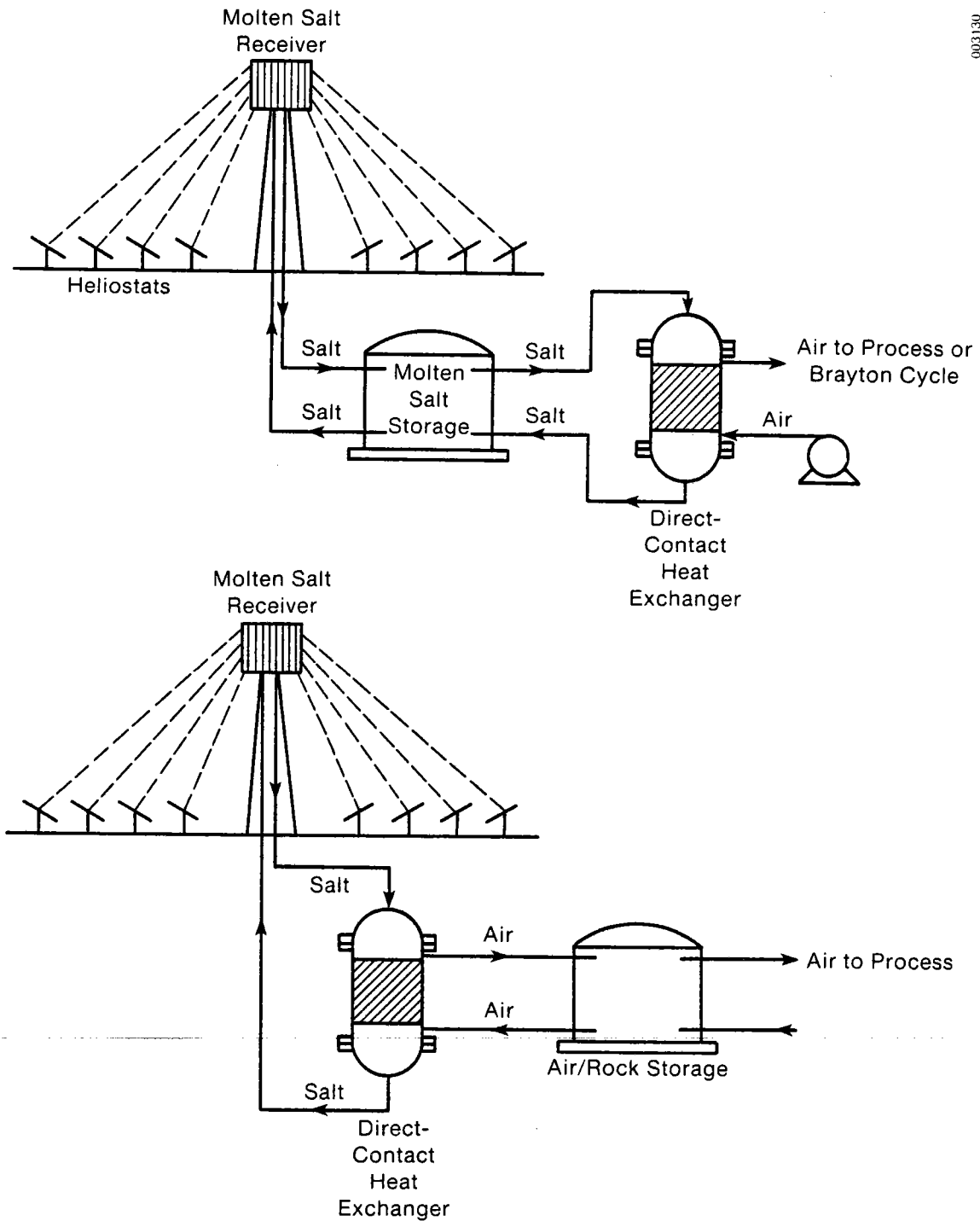


Figure 1-4. Applications of Direct-Contact Heat Exchangers



The objective of the present work is threefold: (1) to experimentally determine the heat-transfer coefficients in direct-contact heat exchange between molten salt and air, (2) to calculate these heat-transfer coefficients based on the mass-transfer analogy and compare them with the experimental data, and (3) to analyze the economics of this system by using the experimental data and comparing DCHX with conventional finned-tube heat exchangers. In general, we want to determine if, and in what applications, DCHX is a cost-effective technology.

In the following sections, we describe calculations of the heat-transfer coefficient based on the mass-transfer analogy; describe the experimental apparatus, methods, and results; compare the results with the calculated values; and, finally, describe an economic analysis that compares the cost effectiveness of DCHX and finned-tube heat exchangers in several applications.

## SECTION 2.0

## THE HEAT-TRANSFER/MASS-TRANSFER ANALOGY

The dimensionless heat-transfer coefficient (Stanton number) may be related to the dimensionless mass-transfer coefficient (Sherwood number) (Kreith 1976) by

$$\frac{h}{GC_p} = \frac{k_g RTP_{BM}}{VP}, \quad (2-1)$$

which is based on the Reynolds analogy and holds only if the Prandtl number (Pr) and the Schmidt number (Sc) both equal unity as shown here:

$$Pr = \frac{\mu C_p}{k} = 1 = \frac{\mu}{\rho D} = Sc. \quad (2-2)$$

In the case where Eq. 2-2 does not hold, heat transfer can often be related to mass transfer by

$$\frac{h}{GC_p} Pr^{2/3} = \frac{k_g RTP_{BM}}{VP} Sc^{2/3} \quad (2-3)$$

from which we can calculate the heat-transfer coefficient

$$h = \left(\frac{Sc}{Pr}\right)^{2/3} \frac{GC_p}{\left(\frac{VP}{k_g RTP_{BM}}\right)} \quad (2-4)$$

For a packed column, transfer coefficients are commonly presented as volumetric coefficients by multiplying the surface coefficients by the interfacial surface area per unit volume  $a$

$$ha = \left(\frac{Sc}{Pr}\right)^{2/3} \frac{GC_p}{\left(\frac{VP}{k_g a RTP_{BM}}\right)}. \quad (2-5)$$

The denominator in parentheses in Eq. 2-5 has dimensions of length and is called the height of a transfer unit  $H_d$ . Correlations of mass transfer are often expressed in terms of  $H_d$ . Fair (1972) gives such a correlation expression for  $H_d$  for packed columns

$$H_{g,d} = \frac{\phi Sc_g^{1/2} d_t^n}{(Lf_1 f_2 f_3)^m}, \quad (2-6)$$

and

$$H_{l,d} = \phi C_f (Sc_l)^{1/2} \quad (2-7)$$

for the gas side and liquid side, respectively. Note that Eqs. 2-6 and 2-7 are dimensional. Dimensions of  $H_{g,d}$  are in  $\text{ft}^*$ ,  $L$  is in  $\text{lbm/h ft}^2$ , and  $d_t$  is in  $\text{ft}$ . We can then calculate the gas side and liquid side heat-transfer coefficients from

$$h_{ga} = \frac{Sc_g}{Pr_g}^{2/3} \frac{C_p G}{H_{g,d}} \quad (2-8)$$

$$h_{la} = \frac{Sc_l}{Pr_l}^{2/3} \frac{C_l L}{H_{l,d}} \quad (2-9)$$

The overall volumetric heat-transfer coefficient is then calculated from

$$Ua = \frac{1}{h_{ga}} + \frac{1}{h_{la}}^{-1} \quad (2-10)$$

The value of the parameters  $m$ ,  $n$ ,  $\Psi$ ,  $\phi$ , and  $C_f$  in Eqs. 2-8 and 2-9 may be found in Table 2-1. The parameters  $f_1$ ,  $f_2$ , and  $f_3$  are functions of the liquid viscosity, density, and surface tension, respectively, and are defined as

$$f_1 = \mu_l^{0.16} \quad (2-11)$$

$$f_2 = \rho_l^{-1.25} \quad (2-12)$$

$$f_3 = (\sigma_l/72.8)^{-0.8} \quad (2-13)$$

Dimensions are:  $\mu_l$  ( $\sim\text{cp}$ ),  $\rho_l$  ( $\sim\text{g/cm}^3$ ),  $\sigma_l$  ( $\sim\text{dyne/cm}$ ).

Experimental conditions can then be used to calculate the heat-transfer coefficient based on the heat-transfer/mass-transfer analogy. The air and salt inlet and outlet temperatures determine all property values. The air and salt flow rate and column diameter determine  $G$  and  $L$  for Eqs. 2-8 and 2-9, respectively. For the experimental apparatus it will be necessary to use Table 2-1 data for the 1-in. Raschig ring packing (because there is not data for 0.5-in. rings) even though the experiment used 0.5-in. Raschig rings. Extrapolation from the 1-in. to 0.5-in. rings from the 1-in. and 2-in.-ring data would be nothing more than guesswork. However, since  $\Psi$  nearly halved in changing from 2-in. to 1-in. rings, some decrease should be expected in changing from 1-in. to 0.5-in. rings. This, in turn, increases the gas side heat-transfer coefficient. Thus, using  $\Psi$  for the 1-in. rings should give conservative values of heat-transfer coefficients. We also need to estimate the percentage of flooding to determine  $\phi$  and  $C_f$ . Constant values of  $\phi = 110$ ,  $\phi = 0.048$ , and  $C_f = 1$  were used. We determined the property values as discussed in Appendix A. Figure 2-1 gives results for air and salt flows and temperatures typical of the experimental apparatus.

\*See Nomenclature for conversion to SI units.

**Table 2-1. Parameters for Packed-Column Heat and Mass Transfer<sup>a</sup>**

	Raschig Rings		Berl Saddles	
	1-in.	2-in.	1-in.	2-in.
m	0.6	0.6	0.5	0.5
n	1.24	1.24	1.11	1.11
ψ				
40% flood <sup>b</sup>	110	210	60	95
60% flood	105	210	60	95
80% flood	80	-- <sup>c</sup>	--	--
φ				
L = 2450	0.045	0.059	0.032	--
L = 4900	0.048	0.065	0.040	--
L = 24,500	0.048	0.090	0.068	--
L = 49,000	0.082	0.110	0.090	--
C <sub>f</sub>				
<50% flood	1.00	1.00	1.00	1.00
60% flood	0.90	0.90	0.90	0.90
80% flood	0.60	0.60	0.60	0.60

<sup>a</sup>Fair 1972.

<sup>b</sup>Flooding is defined as a column pressure drop of 1.5 in. (water column) per foot of bed height.

<sup>c</sup>Data not available or extrapolated.

The film coefficient on the gas side is much smaller than that on the liquid side, and, therefore, the overall coefficient Ua very nearly equals h<sub>g</sub>a. From Eq. 2-6 and 2-8 we see that

$$Ua \sim \frac{m}{a} \cdot \frac{m}{s} \cdot 0.6 \quad (2-14)$$

It will be useful to compare the exponents in Eq. 2-14 with the experimental results. In addition to comparing the relative magnitudes of the calculated and experimental results, comparing the trends is important to determine whether the transfer phenomena are actually equivalent.

The range of experimental parameters (air flow and salt flow) is restricted (see Section 3.4). Within this range we should expect heat-transfer coefficients Ua from about 1000 to 3250 W/m<sup>3</sup> °C.

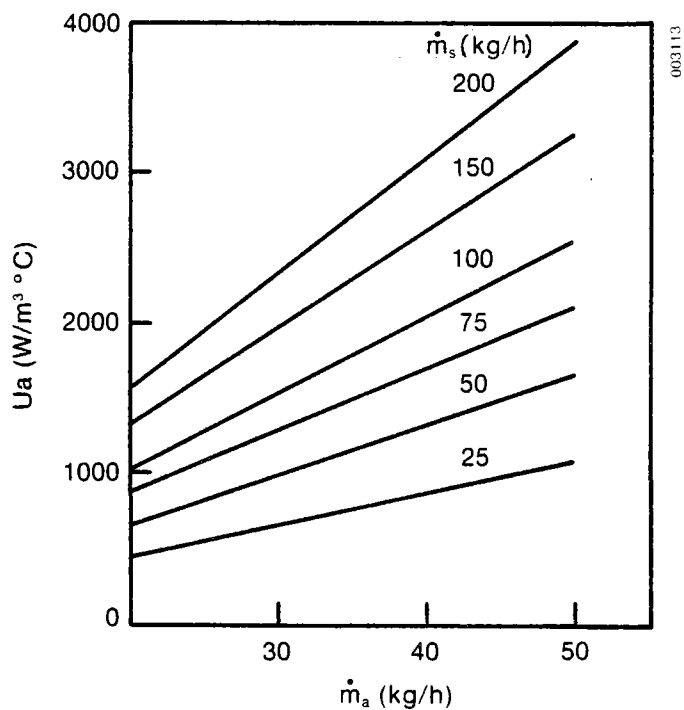


Figure 2-1. Overall Volumetric Heat-Transfer Coefficients Based on Mass-Transfer Data

## SECTION 3.0

### EXPERIMENTAL MEASUREMENTS OF VOLUMETRIC HEAT-TRANSFER COEFFICIENTS

#### 3.1 PURPOSE

As previously mentioned, there are uncertainties associated with calculating the heat-transfer coefficients from mass-transfer data. In addition, there are mechanisms of heat transfer for which no mass-transfer data exist. Therefore, we have developed an experimental program to determine actual volumetric heat-transfer coefficients in direct-contact heat exchange between air and molten salt. Using these data to determine the economic value of DCHX should give us more confidence in the results than if only the calculated heat-transfer values were used.

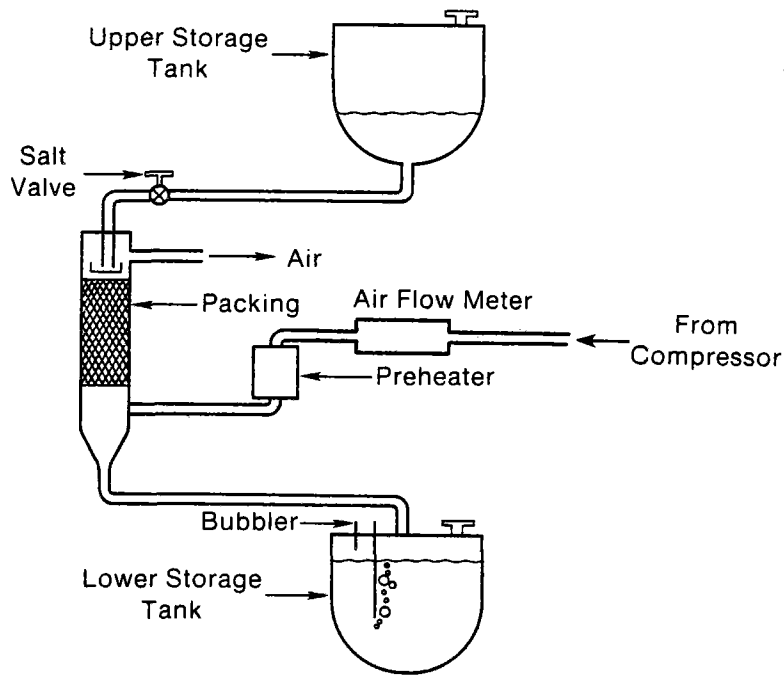
#### 3.2 DESCRIPTION OF THE APPARATUS

A flow diagram of the experimental apparatus is given in Figure 3-1, a detailed diagram of the packed column is shown in Figure 3-2, and a photograph of the apparatus is shown in Figure 3-3. The test loop is a batch operation with regulated air pressure on the upper tank providing regulated salt flow through the salt valve. The upper tank is filled with molten salt and pressurized to approximately 50 kPa. In this way, the salt flow is affected minimally by loss of salt head in the upper tank. The salt flows through the salt valve into the top of the column and into a salt distributor (a can with three holes in its bottom) that distributes the salt uniformly over the top of the bed. Salt flows from the salt inlet pipe directly into the distributor where it flows out the three holes. The distributor is slightly smaller than the column inside diameter, allowing air to flow in the resulting annulus.

The packing bed is supported by a gas-injection support plate that allows the salt to flow downward while providing a uniform air distribution at the bottom of the packing. After the air passes up through the bed, it flows around the annular gap between the salt distributor and the column inside diameter. The air then flows through a wire-mesh mist eliminator that removes any small salt droplets present before the air flows out of the column. Salt flowing out of the bottom of the bed is collected at the bottom of the column and flows to the lower salt tank.

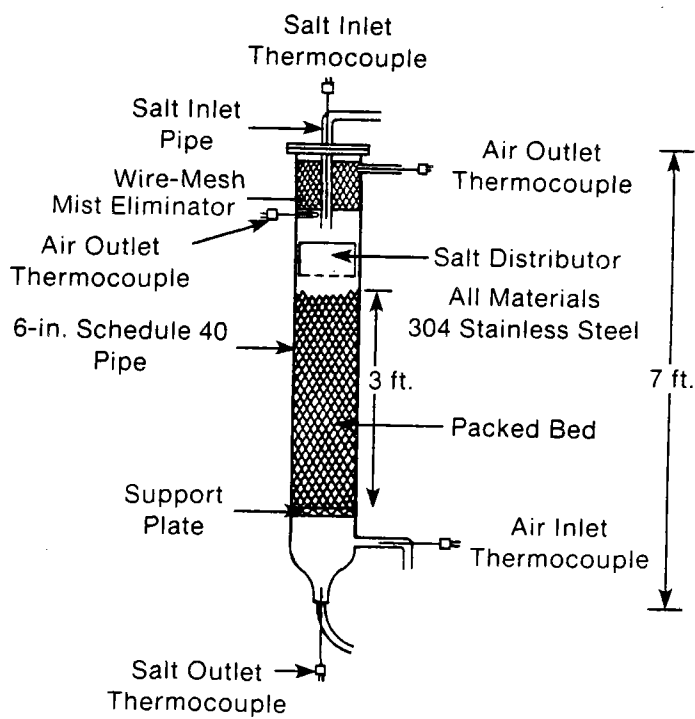
The column size used in this experiment is typical of pilot-scale studies. We determined the column design (size, distributors, bed height, packing size) with the assistance of Norton Chemical Company, Rolling Meadows, Ill. The entire test loop, with the exception of the salt valve, is constructed of 304 stainless steel. The salt valve is 316 stainless steel.

We tested two types of commercially available packing: stainless Raschig rings, and stainless Pall rings (see Figure 1-2). Data on the Raschig rings were useful because of the large amount of mass-transfer data available for them. Supplemental data on the Pall rings were taken because the Norton Chemical Company determined that Pall rings would be the most effective packing for heat-transfer duty. For proper liquid distribution, a general guideline



003127

Figure 3-1. Flow Diagram of DCHX Test Loop



003128

Figure 3-2. Details of the DCHX Packed Column

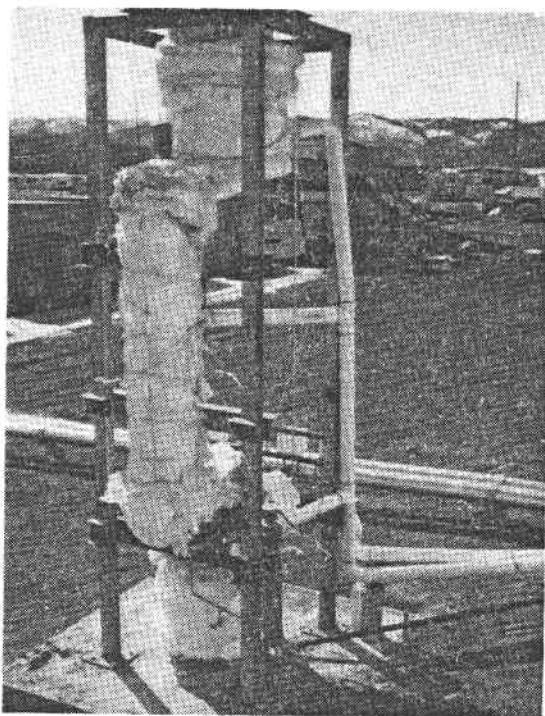


Figure 3-3. Photograph of the DCHX Test Apparatus

(430°F). The nominal molar composition of the salt is 43% potassium nitrate and 57% sodium nitrate. Although the melting point is listed as 222°C by the manufacturer, most of the salt melts in the 240°-305°C range, according to differential scanning calorimetry tests. Since this high melting point caused considerable problems in operation (see Section 3.5), a salt with a lower melting point was used for most of the tests. This salt was Partherm 290 with a molar composition of 40% sodium nitrite, 52% potassium nitrate, and 8% sodium nitrate. The melting point of Partherm 290 is listed as 143°C (290°F) by the manufacturer. One would assume that considerable melting does not occur until approximately 200°C for this salt.

### 3.3 INSTRUMENTATION

Primary instrumentation is shown in Figures 3-1 and 3-2. Air flow rate is measured by an inline mass flow transducer manufactured by Datametrics, Inc.

A bubbler system determines the salt flow rate by continuously monitoring the level of salt in the lower salt tank. This system consists of a tube that passes through the top of the tank to within a few centimeters of the tank bottom and a similar tube short enough so its end is always above the salt surface. By measuring the pressure required to force a bubble of air out the bottom of the long tube, one can determine the salt depth because it determines the pressure head at the end of the long tube. If the lower tank is pressurized, this pressure is sensed by the short tube and subtracted from the pressure at the long tube. The major advantage of this type of system is that molten salt does not come into contact with any parts of the flow measuring



system. The output of the bubbler is proportional to the salt depth, and differentiating this output gives the salt flow rate.

The lower tank was calibrated by filling it with water in 5-L increments and recording the bubbler voltage output. In this way we could directly measure the liquid flow rate because mass flow rate determined by this type of measurement is independent of liquid density. When attempting to measure the salt depth, one must be sure that the salt is completely molten and free of entrained air bubbles.

All thermocouples were Chromel-Alumel (type K). A probe inserted into the vertical portion of the pipe from the upper tank measured the salt inlet temperature (see Figure 3-2). The probe should be an accurate measure of salt inlet temperature since it is totally immersed in salt just before it flows into the salt distributor. This temperature was typically within 2°C of the upper-tank salt temperature.

A probe inserted in the pipe leading out of the bottom of the column measured the salt outlet temperature. We inserted the probe just to where the cone at the bottom of the column begins to expand. The probe was exposed to rivulets dripping from the packing support plate and is the best compromise for measuring salt outlet temperature. Constraints on this measurement include the trace heating on the column wall, which could affect the temperature of salt flowing along the wall, and air entering the column at a lower temperature than the salt leaving the column, which could reduce the outlet salt temperature reading if the probe were inserted further into the column. We observed the responses of this probe to sudden changes in the salt flow, air flow, and air inlet temperature and determined that the probe gives a good indication of salt outlet temperature.

A probe inserted into the horizontal portion of the air inlet pipe measured the air inlet temperature, sensing the temperature of the air about 20 cm from the column. A probe inserted through the column just below the mist eliminator measured the air outlet temperature. Secondary measurements included upper-tank salt and surface temperatures, lower-tank surface temperature, column surface temperature, bed temperature, and the pressure differential between the preheater outlet pipe and the column air outlet pipe.

Operation of the primary thermocouples was checked by placing the probes in condensing steam at local atmospheric pressure (622 mm Hg) corresponding to a saturation temperature of 94.3°C. The five primary probes read 94.4°, 94.7°, 95.1°, 94.2°, and 95.1°C for the salt in, salt out, air in, air out (column), and air out (outlet pipe) temperatures, respectively.

Readings from the outlet air probe indicated a close approach (~10°C) to the salt inlet temperature. This implies that either the heat exchanger is very effective or that some of the salt flowing in the top of the bed is carried up beyond the distributor and contacts the probe causing it to read too high. Any salt trapped in the mist eliminator could also drip onto this probe. To resolve this we inserted a second air outlet probe through the air outlet pipe to just inside the mist eliminator (see Figure 3-2). This probe read about 7°C lower than the probe near the mist eliminator. Pulling the probe out about 2 cm so it was not inside the mist eliminator increased the difference

to about 14°C. With the probe pulled out to about 20 cm from the mist eliminator the discrepancy was about 50°C. Therefore, a large temperature gradient exists in the air outlet port area, and it is difficult to measure the air outlet temperature. For other reasons (see Section 3.6) we used the temperature measured by the probe inserted in the column just below the mist eliminator as the actual air outlet temperature.

Data were recorded by a Hewlett-Packard Model 85 computer that gave printed, displayed, and plotted information. A Leeds and Northrup strip chart also recorded surface temperatures, air flow rate, and bubbler output.

### 3.4 COLUMN SIZING

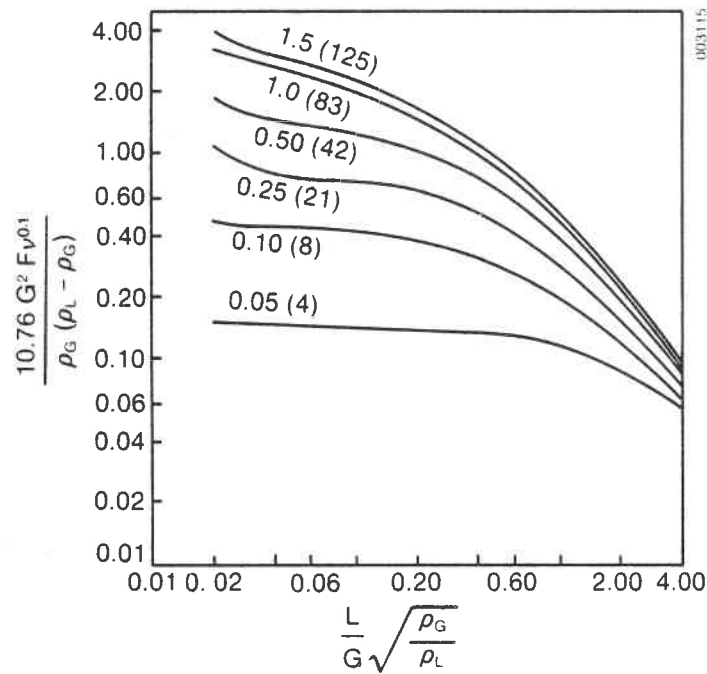
Flooding constraints determine the column design in terms of allowable liquid and gas flow. Flooding occurs when a large quantity of the liquid is entrained with the gas and carried upward with it. This situation is caused by increasing the liquid flow rate at a fixed gas flow rate. Decreasing the gas flow allows more liquid flow before flooding. Flooding produces excessive pressure drop and must be avoided in commercial applications. The generalized pressure drop correlation (Norton Chemical 1977), seen in Figure 3-4, gives this relationship in general terms. This correlation gives lines of constant pressure drop across the column bed as a function of flow rates and properties of the gas and liquid. When this correlation is made specific to the experimental design with air and molten salt and for 0.5-in. Raschig rings, the pressure drops shown in Figure 3-5 results. Also shown in Figure 3-5 are the limits of salt flow and air flow for the apparatus and the points where actual data were taken.

Table 3-1 gives nominal design values for the experimental apparatus. We chose the maximum operating temperature of 350°C because common nitrate salts do not cause excessive corrosion with the stainless steel alloys at this temperature. We felt that from what is known about materials compatibility, adequate operating time could be expected from the apparatus by limiting operation to 350°C.

**Table 3-1. Nominal Column Operating Conditions**

Salt inlet temperature	350°C
Air inlet temperature	200°C
Salt flow rate	$\dot{m}_s = 80 \text{ kg/h}$ $L = 4390 \text{ kg/h m}^2$
Air flow rate	$\dot{m}_a = 40 \text{ kg/h}$ $G = 2190 \text{ kg/h m}^2$
Heat duty	$Q = 2 \text{ kW}$

It is clearly necessary to maintain all surfaces with which the salt comes in contact at a temperature above the freezing point of the salt, including the exterior surface of the column. In practice, the column surface would probably be heated only for start-up; and when operating conditions were reached, the heat tracing would be turned off. Then, the insulation applied to the outside surface of the heat exchanger would control the heat losses. In this experimental apparatus we left the heat tracing on during heat-transfer experiments



**Figure 3-4. Generalized Pressure Drop Correlation.**  
 Parameter on curves is pressure drop in inches of water per foot of bed height; figures in parentheses are millimeters of water per meter of bed height.

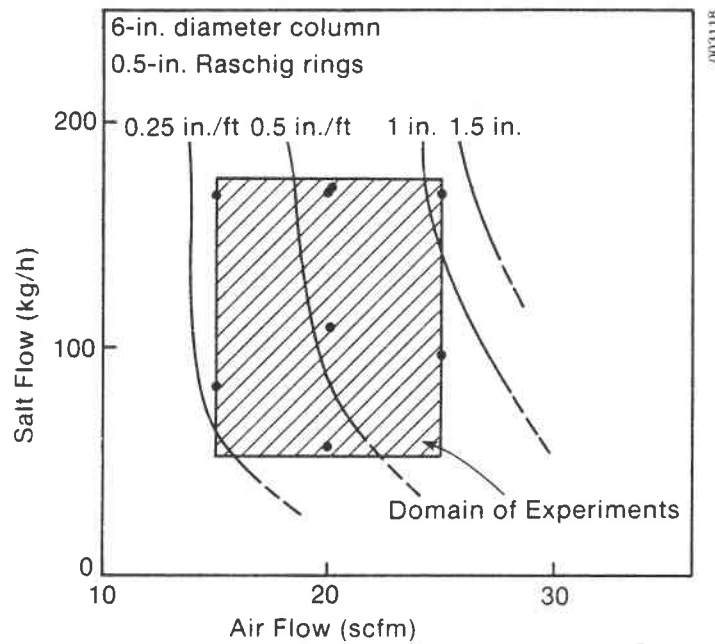


**Figure 3-5. Pressure Drop for Experimental Apparatus.**  
 Parameter on curves is pressure drop in inches of water per foot of bed height.

to control the tendency of cold spots to form frozen salt, which blocks the column. In addition, the heat tracing was set to maintain the column surface near the operating temperature to minimize start-up transients and to act as a guard heater, minimizing losses from the salt to ambient.

Heat tracing required to initially bring the loop up to operating temperature and to maintain this temperature was a high-temperature tracing supplied by Nelson Electric (type A-846K-016-07). The tracing has a stainless steel shell (0.25-in. outside diameter) with nichrome wire inside that is protected from the shell with a refractory insulation. This heat tracing was secured to all exterior surfaces of the test loop (including both tanks, piping, and the column) with baling wire supplied with the heat tracing. Approximately 50 m of the heat tracing was required to provide adequate heating. We then insulated the test loop with a Johns-Manville Cerawool blanket to a thickness of approximately 15 cm.

### 3.5 OPERATIONAL PROBLEMS

Most operational difficulties were caused by localized cold spots in the transfer piping. It was difficult to apply the heat tracing, because it was rather stiff and could not be easily formed to fit all contours uniformly especially near valve bodies, on the transfer pipes, and on the bottom conical portion of the column. We alleviated some of these problems by replacing the original salt with one having a lower melting point (143°C versus 221°C for the first salt).

Only one materials-related failure occurred. The heat tracing overheated on the connecting tube about 30 cm from the upper tank, corroding the tube, and the entire contents of the upper tank leaked out. On examination we found the tubing had a dark brown discoloration about 3 cm long on either side of the hole. We subsequently replaced all the tubing with some that had a larger diameter and a heavier wall (0.75-in. schedule 40 pipe with a 0.113-in. wall versus 0.5-in., 0.035-in.-wall tubing). Using a larger diameter tubing allowed better application of the heat tracing because it was easier to form the tracing to the contours of the larger tubing. In addition, the salt tends to freeze more easily in small-diameter tubing. Most operational difficulties were eliminated after installation of the larger-diameter tubing.

A brownish residue collected in the bottom of the upper salt tank. Analysis of this residue is given in Table 3-2 along with an analysis of the as-received salt. It appears that at some point in the loop, the salt is reacting with the containment materials; that even at 350°C, long life could be a problem; or that temperatures in parts of the test loop are substantially above 350°C. Operational problems resulted, as this viscous residue tended to plug the salt valve, making it difficult to maintain a constant salt flow. Foreign particulate matter also became trapped in the valve orifice. These particles were very hard and brittle (similar to small pebbles) and were either related to the viscous residue or in the salt as delivered.

Table 3-2. Analysis of Upper Tank Residue

Residue	Salt after ~3600 h	As-received Salt
% Fe 0.70	--- <sup>a</sup>	--
% Mg 1.50	--	0.005
% Ca 0.50	0.003	0.003
% Ti 0.03	--	--
% Si 1.0	---	--
% Al 0.2	--	--
ppm Mn 100	--	--
B 20	--	--
Ba 30	--	--
Cr 70	5	--
Cu 15	---	--
Mo 15	--	--
Ni 150	---	--
Pb 20	--	--
Sr 30	---	--
V 20	--	--

<sup>a</sup>None detected.

The apparatus shown in Figure 3-1 is somewhat simplified from the original design, which had two features that caused operational problems and were ultimately abandoned. The salt valve originally was electrically actuated and could be operated remotely from the control room. This provided a way to control the salt flow as the salt head in the upper tank was reduced. Unfortunately, the valve did not operate as smoothly as required, and, if salt froze in the valve, it was difficult to diagnose the lack of salt flow because of the remote location of the actuator. Finally, the weight of the entire valve/actuator assembly caused one of the tubing welds to break. We replaced the valve with a manual bellows valve, and the pneumatic system described previously provided good salt flow control.

The second feature we abandoned was a pneumatic system for transferring the salt in the lower salt tank to the upper salt tank. The system involved a pipe from the lower tank to the upper tank and associated valves for isolating the lower tank. Applying air pressure to the lower tank forced the salt into the upper tank. Problems with this system were primarily related to salt freezing in the return line; plus, the extra valves provided more locations where we could not apply the heat tracing. We removed the additional valves when we replaced the small-diameter tubing, and we manually transferred the salt to the upper tank thereafter.

### 3.6 HEAT-TRANSFER MEASUREMENTS AND PROCEDURES

Using the inlet and outlet salt and air temperatures and the salt and air flow rates, we can determine the rate of heat transfer from

$$Q_s = \dot{m}_s C_s (T_{si} - T_{so}) , \quad (3-1)$$

$$Q_a = \dot{m}_a C_{pa} (T_{ao} - T_{ai}) . \quad (3-2)$$

Equation 3-1 gives the rate of heat transfer from the salt, and Eq. 3-2 gives the rate of heat transfer to the air. We determined the specific heat for the air and the salt using the method described in Appendix A. A comparison of  $Q_s$  and  $Q_a$  gives a quantitative measure of the quality of the heat-transfer data since in the absence of heat losses and measurement errors we would have  $Q_s = Q_a$ . Therefore, we will refer to the absolute value of the quantity  $100(1 - Q_s/Q_a)\%$  as the heat balance for the experiment.

We can then calculate the volumetric heat-transfer coefficient from

$$Ua = \frac{Q}{V_p \Delta T_m} , \quad (3-3)$$

where  $V_p$  is the volume of the packing bed [15 cm (inside diameter) x 0.914 m = 0.0167 m<sup>3</sup>] and  $\Delta T_m$  is the log-mean temperature difference, defined as

$$\Delta T_m = \frac{(T_{si} - T_{ao}) - (T_{so} - T_{ai})}{\ln\left(\frac{T_{si} - T_{ao}}{T_{so} - T_{ai}}\right)} . \quad (3-4)$$

The value of  $Q$  in Eq. 3-3 can be either  $Q_s$  or  $Q_a$ , and the error in  $Ua$  is therefore equal to the heat balance for the experiment.

From Eq. 3-4 it is clear that for a close approach ( $T_{ao} \approx T_{si}$ ), which is typical of these experiments, large errors in  $\Delta T_m$  and therefore in  $Ua$  can result. Table 3-3 demonstrates this from the baseline of actual measured data for one run; the value of  $T_{ao}$  was perturbed to show the effect on  $Q_a$  and  $Ua$ . This shows that for values of  $T_{ao}$  lower than the measured value (typical of the probe in the air outlet line), the heat balance is poor. For values of  $T_{ao}$  larger than the measured value at the bottom of the mist eliminator, the heat balance is good, but  $Ua$  increases very rapidly as  $T_{ao}$  approaches  $T_{si}$ . For a 5.2°C increase in  $T_{ao}$ ,  $Ua$  increases by 40%.

Although the thermocouple should not generate errors greater than  $\pm 1^\circ\text{C}$  (see Section 3.3), placing the air outlet probe where it is influenced by salt draining from the mist eliminator, heat tracing on the column walls, etc., could cause large errors. The solution is to totally separate the two phases to eliminate the influence of salt in the measured air temperature and at the same time to place the probe close enough to the top of the bed to get a true

Table 3-3. Measured Data Showing Effect on  $Q_a$  and  $U_a$ 

	$T_{ai}$	$T_{ao}$ (°C)	$T_{si}$	$T_{so}$	$\dot{m}_s$ (kg/h)	$\dot{m}_a$	$Q_s$ (W)	$Q_a$ (W)	$U_a$ $W/m^3 \text{ } ^\circ C$
baseline	193.7	334.8	341.9	309.9	167.8	50.9	2305	2065	3536
	↓	294.0	↓	↓	↓	↓	↓	1468	1791
		300.0						1556	1895
		340.0						2141	4966
	↓	341.8	↓	↓	↓	↓	↓	2167	8389

air outlet temperature. Based on the two air outlet temperature probes (one inserted through the column wall just below the mist eliminator and the other inserted through the knockout pot just inside the mist eliminator), it appears that one probe may read slightly high because of entrained salt and that the other may read lower by a few degrees. The best temperature measurement to use, therefore, is the one just below the mist eliminator.

Experimentally, it is possible to vary the salt flow rate, the air flow rate, and the salt and air inlet temperatures. The last two variables are of secondary importance (as long as the air inlet temperature is above the salt freezing point), so we did not vary them in any systematic way. The salt flow rate was varied from 50 to 200 kg/h, and the air flow was varied from 30 to 50 kg/h (see Figure 3-5). We could attain higher salt flow rates, but this would result in run times too short to establish steady conditions--a crucial requirement for good data; i.e., small values of the heat balance. Figure 3-5 shows that air flow rates much larger than 50 kg/h (~25 scfm) produces column flooding.

The system was not temperature-cycled but was left at operating temperature for about six months continuously with the exception of downtime for repairs, as described previously. To minimize the time required to reach steady state and to minimize losses, we set the heat tracing so the bed temperature was fairly close to the upper tank salt temperature. Pressure was applied to the upper tank from the regulated air supply, and the salt valve was opened. To achieve a constant salt flow rate, as indicated by the bubbler output trace, generally required 20 minutes. (As long as nothing lodged in the valve, this flow rate was steady until the upper tank was empty.) We then set the air flow to the desired value (it was helpful to heat the preheater to about 200°C before turning on the air), and, when steady state was achieved, we could adjust the air flow to a new setting.

Examination of the data indicated that the best heat balances were achieved when the salt flow was the most uniform and when no adjustments of the salt valve or tank pressure were necessary. A typical run of two hours provided data on one salt flow rate and five air flow rates.

3.7 RESULTS AND DISCUSSION

Experimental data for Raschig rings are presented in Figure 3-6 in the form of volumetric heat-transfer coefficient versus air flow rate with salt flow as a parameter. The data are also shown in Table 3-4 with the heat-transfer coefficient calculated from the mass-transfer analogy, Eqs. 2-6 through 2-9.

The heat-transfer coefficients do not appear to depend on salt flow rate, as all the data for  $\dot{m}_a \approx 40$  kg/h and for  $57 < \dot{m}_s < 170$  kg/h vary by only a few percentage points. The variation with air flow is relatively strong--a best fit produces

$$U_a = 21.1 \dot{m}_a^{1.28} \tag{3-5}$$

where  $\dot{m}_a$  is in kg/h and  $U_a$  is in  $W/m^3 \text{ } ^\circ C$ . This is clearly at variance with Eq. 2-14.

As shown in the last column of Table 3-4, heat-transfer coefficients calculated from mass-transfer data underestimate measured heat-transfer coefficients except at large salt flows. Because the experimental data do not correlate with Eq. 2-14, it is doubtful that using the mass-transfer/heat-transfer analogy will work. Apparently, the heat-transfer mechanism does differ significantly from the mass-transfer mechanism, as discussed in Section 1.0.

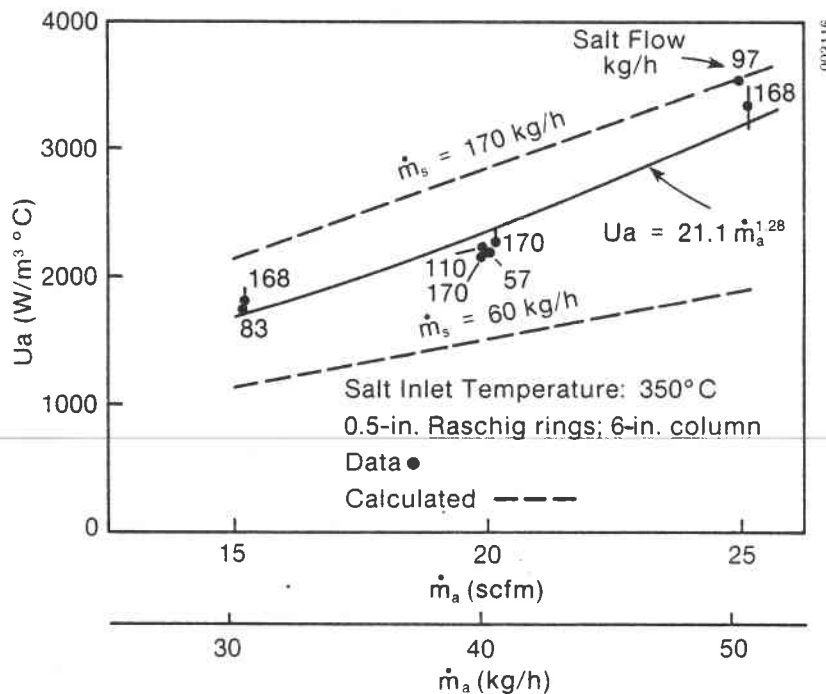


Figure 3-6. Overall Volumetric Heat-Transfer Coefficients Based on Experimental Data



Table 3-4. Heat-Transfer Data and Comparison with Mass-Transfer Calculations

Salt Inlet Temperature (°C)	Air Flow (kg/h)	Salt Flow (kg/h)	Measured $U_a$ (W/m <sup>3</sup> °C)	Heat Balance (±%)	Calculated $U_a$ (W/m <sup>3</sup> °C)
342	30.8	168	1820	3	2171
348	30.9	83	1771	2	1429
341	40.7	171	2252	6	2896
353	40.5	57	2203	3	1478
349	40.3	170	2164	4	2854
348	40.2	110	2228	1	2189
348	50.5	96	3520	5	2535
342	50.9	168	3351	5	3574

Data for the Pall rings are compared with the Raschig ring data correlation, Eq. 3-5 in Figure 3-7. Data were for a salt flow rate of only ~130 kg/h; we did not test the dependence of heat transfer on salt flow rate. The three data points fall fairly close to the Raschig ring curve, although the point for the highest air flow is somewhat below (~20%) the curve.

Overall heat-transfer coefficients calculated from mass-transfer data are shown in Figure 3-6 for two salt flow rates, 170 and 60 kg/h. These results further demonstrate the lack of sensitivity to salt flow rate for the heat-transfer data compared to the mass-transfer data. There are several possible explanations as to why the heat-transfer data do not depend on salt flow rate while the mass-transfer data do, as explained in Section 1.0. These explanations are the (1) different wetting characteristics of the packing by the salt, (2) heat conduction through the metal wall of the packing, and (3) radiation heat transfer.

If the salt totally wets the packing, any increase in salt flow beyond some minimum will not provide more heat-transfer surface area per volume of packing, causing the volumetric heat-transfer coefficient to be insensitive to salt flow. Since  $U_a \approx h_g a$ , the volumetric coefficient  $U_a$  may only be affected by changing the gas-side film coefficient  $h_g$  or the surface area per unit volume  $a$ . This is consistent with the similarity between the Pall ring data and the Raschig ring data (Figure 3-7). From Figure 1-3 one can see that the two packing types should provide similar surface areas per unit volume since the only difference is that the Pall rings have the spokes punched in from the periphery of the ring.

Peters and Timmerhaus (1980) give surface areas per unit volume for several types and sizes of packings. For the 0.5-in. metal Raschig ring (with 0.06-in. wall), approximately 118 ft<sup>2</sup> of surface are provided per ft<sup>3</sup> of packing volume. For the Pall ring, the value is 104 ft<sup>2</sup>/ft<sup>3</sup>. The two types of packing provide similar heat-transfer areas and, therefore, if fully wetted by the salt, should exhibit about the same heat-transfer performance.

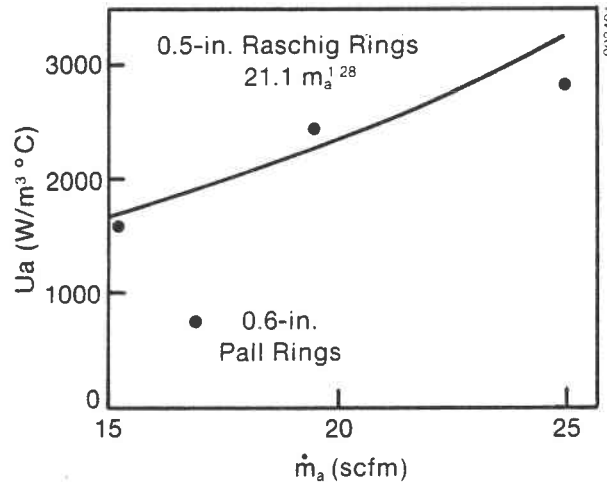


Figure 3-7. Comparison of Measured Heat-Transfer Coefficients For Pall Rings and Raschig Rings

On the other hand, if conduction heat transfer in the packing is important, then it would not be important how much of the surface of the packing is wet by the salt because heat could then be transferred from the dry areas of the packing to the air.

A better understanding of the heat-transfer mechanism is required. By performing tests at various temperatures with liquids having various wetting properties and with packings of various thermal conductivities and surface areas, it should be possible to separate the different heat-transfer mechanisms.

Overall system pressure drop is plotted in Figure 3-8. Recall that this is a measure of the differential pressure from the column air inlet pipe to the column air outlet pipe. Therefore, it includes not only pressure drop across the bed (Figure 3-5), but expansion and contraction losses at the column inlet and column outlet and loss across the air distributor, salt distributor, and the mist eliminator. We took additional pressure drop data with zero salt flow to determine the contribution of all these column components. These data allow only a qualitative assessment of the bed pressure drop because it is only about 30% or 40% of the measured system pressure drop. We could not find a satisfactory method for measuring bed pressure drop because of the difficulties associated with isolating the high-temperature salt from a pressure-sensing port or isolation diaphragm.

The data in Figure 3-8 clearly show the benefits associated with using Pall rings. At a given air flow the overall system pressure drop for the Pall rings is about half that of the Raschig rings. From Figure 3-4 we see that constant bed pressure drop,  $G \sim \sqrt{F}$ , in the region of the map where the  $\Delta p$

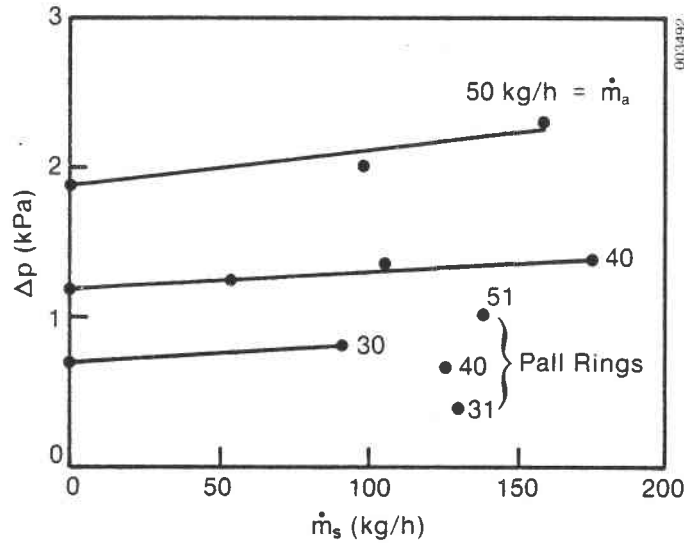


Figure 3-8. Overall System Pressure Drop

lines are level. Since the packing factor  $F$  for Pall rings is about 0.17 that of Raschig rings, we could operate with approximately  $\sqrt{6} = 2.4$  times as much air flow with Pall rings compared to Raschig rings in the experimental column. The ratio for large (2-in.) packing is close to 2, so we could operate with about 41% more air in a large column with Pall rings than with Raschig rings. From Eq. 3-5 the Pall rings could provide about  $1.41^{1.28} = 1.55$  more heat transfer per unit volume than Raschig rings in a large column. Extrapolation of Eq. 3-5 to such large air flows should be tested experimentally to determine if flooding is approached. This would most likely cause the volumetric heat transfer to fall below that predicted by Eq. 3-5.

## SECTION 4.0

## ECONOMIC ANALYSIS

## 4.1 PURPOSE

With experimental and calculated values for the heat-transfer coefficient, we can now determine the economic value of DCHX. Rather than basing economic calculations solely on the mass-transfer data, using actual heat-transfer data should give us more confidence in the results. As explained in Section 4.2, the experimental data cannot be applied directly to a commercial-size DCHX, and, therefore, even these results require some caution in interpretation.

## 4.2 METHOD OF ANALYSIS

The economics of DCHX and finned-tube exchangers are compared by considering all capital and operating costs associated with the heat exchanger. Using the methodology in Appendix B, one can then calculate the annual levelized cost. This is the constant annual cost (in fixed dollars) that, if paid over the lifetime of the heat exchanger, would have a present value equal to the present value of the actual costs incurred over the lifetime of the heat exchanger. In computing one single cost this method can easily consider: escalation rates, depreciation, discount rates, lifetime, and tax rates, among other parameters. Appendix B describes the method and also gives the values for these parameters used in the analysis.

We will assume that only one capital cost is incurred and that the only operating cost is that associated with the power required to pump the air through either heat exchanger. Maintenance costs will be taken as a constant annual cost equal to 3% of the capital cost. With these assumptions and the values of the parameters given in Appendix C, the annual cost may be computed from

$$AC = 0.2299 \times CI + 1.886 \times OM , \quad (4-1)$$

where CI is the capital cost expressed in 1981 dollars and OM is the annual cost of pumping the air, also expressed in 1981 dollars. We will generally give results in the form of AC/Q, which is the annual cost per unit heat transferred in \$/GJ. Note that this is quite close to \$/10<sup>6</sup> Btu transferred.

Considering the pumping cost first, for the cost of electricity given in Appendix B (\$12.89/GJ = \$0.0464/kWh), we see that

$$OM = 1.68 \times 10^{-4} C_f \frac{\Delta p}{\rho} \dot{m}_a \text{ (\$/yr)} , \quad (4-2)$$

which assumes an isentropic efficiency of 0.70 for the compressor, an electrical motor efficiency of 0.96, and a plant capacity factor  $C_f$  of 0.8. We can calculate the pressure drop  $\Delta p$  through the heat exchanger once we know the

air flow rate and the characteristics of the heat exchanger (friction factor versus Reynolds number plot for the finned-tube exchanger and the generalized pressure drop correlation curve for the packed column).

To determine capital cost, we must know the size of the heat exchanger and the materials of construction. The first is determined by the required heat duty, overall heat exchange coefficients, and log-mean temperature differences. Materials of construction are determined by operating temperature and working fluids (see Section 4.3). For consistency, we used the data given by Peters and Timmerhaus (1980) for all the capital costs.

For the finned-tube heat exchanger, the size is best expressed as heat exchange area including fins. Peters and Timmerhaus (1980, p. 669) give a graph of the cost of carbon steel, finned-tube, and floating-head heat exchangers operating at 10 atm. This curve has been generalized to a correlation curve

$$CI = 2051 A_a^{0.6622} \quad (\$) \quad (4-3)$$

that includes a factor of 2.3 for installation cost, a factor of 1.8 for the use of stainless steel in the entire heat exchanger (see Peters and Timmerhaus 1980, p. 677), and a factor of 1.12 to escalate the 1979 cost to 1981 dollars. For atmospheric pressure operation the capital cost is reduced by a factor of 0.92 (Peters and Timmerhaus 1980, p. 673). For materials other than stainless steel the cost is adjusted according to the table given in Peters and Timmerhaus (1980, p. 677), which lists relative cost factors for entire heat exchangers of several different materials of construction. For carbon steel the factor is 0.56; and for Incoloy, it is 1.67. The factor between carbon steel and stainless steel (0.56) is consistent with cost data in Dubberly et al. (1981), which gives 0.60. It is also consistent with a rule-of-thumb (0.5) used by Mercury Fin Tube Products to scale the cost of a stainless steel, finned-tube heat exchanger to a carbon steel unit.

Peters and Timmerhaus (1980, p. 772) also give installed costs for packed towers (excluding cost of packing) as a function of the height and diameter of the column. For a stainless steel column from 1 m to 5 m in diameter, the correlation curve is

$$CI = 10,762 H_d^1.29 \quad (\$) , \quad (4-4a)$$

and for carbon steel it is

$$CI = 2620 H_d^1.34 \quad (\$) , \quad (4-4b)$$

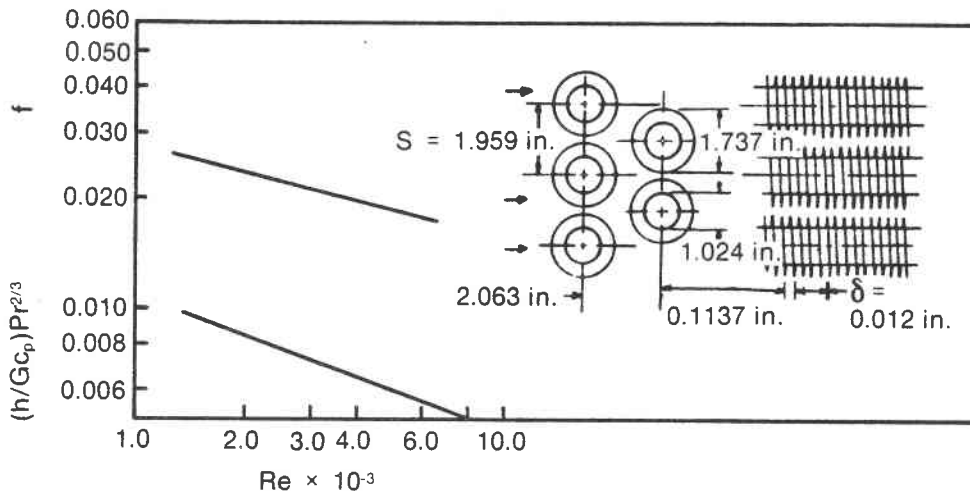
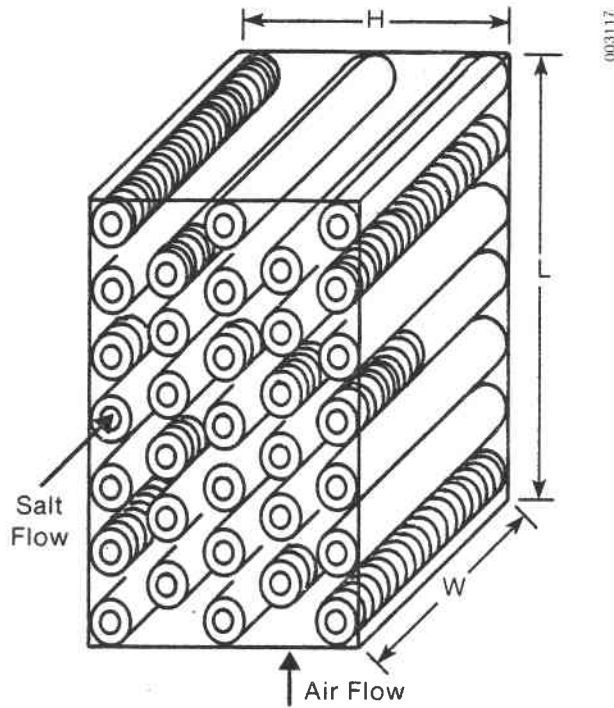
which includes a factor of 1.03 to account for the cost of installing insulation and the same 1.12 factor to escalate costs to 1981 dollars. For operation at pressures other than atmospheric the cost is escalated by the same factor used to rate shell-and-tube heat exchangers (Peters and Timmerhaus 1980, p. 673) applied to the fraction of column cost attributable to the shell, ~55%. Note that we did not increase the cost of the finned-tube heat exchanger to include insulation costs because we assumed that such a unit

would ordinarily be insulated, and the insulation would be part of the 2.3 factor for installation costs. Since packed columns are not ordinarily insulated, we included the factor of 1.03 for the packed-column capital cost calculation. For the high-temperature DCHX a more complex column design required costing of individual components related to the insulation (see Section 4.3).

For the finned-tube heat exchanger we used the characteristics of the heat exchange core, denoted CF-8.8-1.0J by Kays and London (1964), which consists of 1-in. tubes (outside diameter) on 1.96-in. spacing using spiral-wound fins with 8.8 fins/in. and a 0.012-in. fin thickness. Data on the core includes the Colburn  $j$  factor (the heat-transfer coefficient on the air side) and the friction factor as a function of the air-side Reynolds number. The salt-side Reynolds number was chosen as a constant (10,000) because the overall heat-transfer coefficient is not a strong function of the salt-side Reynolds number as long as the salt flow is turbulent. Also, salt-side pumping work is negligible, so we need to consider only the salt-side pressure drop from the standpoint of tube stress at elevated temperatures.

The layout of the core is shown in Figure 4-1. Salt flows through the tubes, and air flows across the finned tube banks (crossflow arrangement). Given the flow rates (determined from the heat duty and terminal temperatures), we can determine the heat exchanger effectiveness and the required number of transfer units (NTU) from equations for crossflow exchangers. Beginning with the lowest air-side Reynolds number for which the heat exchanger core data are given, we can determine the value of  $W$  ( $H$  is arbitrarily set equal to  $W$ ), calculate the air-side heat-transfer coefficient and the fin efficiencies, and then determine the overall heat-transfer coefficient. From NTU we can now calculate the required total heat-transfer surface required, which determines the core dimension in the air flow direction  $L$ , which also determines the core pressure drop. With the surface area and pressure drop we can calculate the cost  $AC$ . This procedure is repeated for increasing air-side Reynolds numbers until a minimum cost results. We restricted the heat-exchanger core to the maximum heat-transfer area ( $900 \text{ m}^2$ ) for which cost data exist in Peters and Timmerhaus (1980). This corresponds to a shell diameter of 2.77 m (9.09 ft) for 4.87-m (16-ft) long, 2.54-cm (1-in.) (outside diameter) tubes. Multiple heat exchangers are specified when heat duties require more than this maximum heat-transfer area.

Optimization of the DCHX is somewhat different because of flooding constraints. Outlet air temperature cannot be specified a priori. Beginning with a column diameter of 1 m (the smallest diameter for which cost data are available), we calculated the volume of packing. (We used the shortest practical column height, equal to the diameter, because this always minimized annual cost. Column diameters larger than the column height produce problems with uniform salt and air distribution in the column.) For an assumed value of the overall heat-transfer coefficient, we determined the log-mean temperature difference, which gives us the air outlet temperature. This determines the air flow rate, and from the generalized pressure drop correlation we can then determine the pressure drop. We rejected diameters that produce operating conditions off the generalized pressure drop map (Figure 3-4). We used a maximum column diameter of 5 m since this is the largest for which Peters and Timmerhaus (1980) give cost data. Knowing the column size and pressure drop, we could calculate the annual cost.



- Tube outside diameter = 1.024 in.
- Fin pitch = 8.8/in.
- Fin thickness = 0.012 in.
- Fin area/total area = 0.825
- Flow passage hydraulic diameter,  $4r_h = 0.01927$  ft
- Free-flow/frontal area,  $\sigma = 0.439$
- Heat transfer area/total volume,  $\alpha = 91.2$  ft<sup>-1</sup>
- Note: Minimum free-flow area is in spaces transverse to flow.

Figure 4-1. Layout of the Finned-Tube Heat Exchanger Core

We repeated the procedure for increasing column diameters giving annual cost as a function of approach temperature (air outlet temperature). The overall volumetric heat transfer is taken as a parameter; for most calculations we used the values  $U_a = 2000, 3000, 4000 \text{ W/m}^3 \text{ }^\circ\text{C}$ . We can then use the experimental values of  $U_a$  or the calculated values of  $U_a$  along with the results of this economic calculation (which also gives sensitivity to  $U_a$ ) to appraise the economic viability of DCHX relative to finned-tube heat exchangers.

#### 4.3 MATERIALS

From exposure tests of up to 4500 hours at temperatures up to about  $600^\circ\text{C}$ , Tortorelli and DeVan (1982) demonstrate that stainless steel alloy 316 oxidizes at the rate of 5 mil/yr or less, typically 2 mil/yr. A 90-mil tube wall thickness, therefore, should be adequate for a 30-year life. Fin material will also have to be stainless steel because of manufacturing constraints and materials compatibility considerations.

For the packed column at  $600^\circ\text{C}$  or lower, we specify stainless steel Pall rings for the packing and a stainless steel column with external insulation. Internal insulation with a liner to contain the salt and support the packing would allow us to use a carbon steel column, greatly reducing the cost. This insulation method has been tested by Martin Marietta (1979) but is not commercially available at this time; therefore, it involves some technical risk. An alternative design that may prove economical at intermediate temperatures is an externally insulated, carbon-steel column with an Inconel liner. This configuration was not examined in this study.

At temperatures above  $600^\circ\text{C}$ , common nitrate heat-transfer salts decompose. SERI, Oak Ridge National Laboratory, and other laboratories are presently researching candidate heat-transfer salts and compatible containment materials at temperatures above  $600^\circ\text{C}$ . Based on state-of-the-art knowledge it appears that Incoloy 800 alloy is a reasonable choice for finned-tube heat-exchanger materials for temperatures  $<800^\circ\text{C}$ .

The DCHX for temperatures  $<800^\circ\text{C}$  consists of an internally insulated, carbon-steel column similar in design to the storage tank described in Martin Marietta (1979). A high-purity (99% alumina) packing is required to resist attack by the salt. To seal the insulating firebrick from the salt, an Inconel liner is necessary. A layer of fiberglass insulation will cover the outside of the column, and aluminum lagging will weatherproof the assembly.

High-purity alumina packing is not commonly available. We determined the cost of this packing from the cost ratio (3:1) between 99% and 57% alumina catalyst support from Norton Chemical Company. To account for unknown manufacturing difficulties that could arise when fabricating saddles from the 99% alumina, a cost factor of 4 (suggested by Norton Chemical Company) was applied to the 1983 second quarter price ( $\$19.80/\text{ft}^3$ , 100  $\text{ft}^3$  order) quoted by Norton Chemical Company, giving an equivalent 1981 cost of  $\$70.49/\text{ft}^3$ . The packing is the major cost item for the DCHX, which suggests that a spray column could be a viable, high-temperature alternative.



The Inconel liner cost was taken from Martin Marietta (1979) who priced an Incoloy liner with a waffled design to accommodate thermal cycling. Since the DCHX does not operate in a cycling mode, the liner can be a simpler design that allows for thermal expansion. Allowing a 2 cost factor between Incoloy and Inconel and a 0.5 factor for a simpler liner design, the cost of the installed liner is  $\$283/\text{m}^2$  internal column area.

The firebricks (Krilite 30) need to be thick enough to allow the carbon-steel column to operate below  $316^\circ\text{C}$  for an internal temperature of  $760^\circ\text{C}$  and to keep thermal losses to less than 1% of the transferred heat. The cost of the firebrick from Martin Marietta (1979) is  $\$809/\text{m}^3$ .

The cost of the carbon-steel shell is calculated in Eq. 4-4b. For the fiberglass outer insulation (sufficient thickness to keep losses to 1% of the transferred heat when the ambient temperature is  $20^\circ\text{C}$  and the carbon-steel column is  $316^\circ\text{C}$ ) Martin Marietta (1979) used  $\$265/\text{m}^3$  of insulation and  $\$25/\text{m}^2$  of aluminum lagging.

Temperatures above  $800^\circ\text{C}$  will most likely require ceramic finned-tube heat exchangers. Although the cost of these ceramic heat exchanger tubes is not prohibitive (most likely less than the cost of higher alloy tubes), fabricating the tubes into a heat exchanger is a relatively unknown art. Therefore, cost projections are difficult. Construction of the packed column, however, would not change drastically for temperatures above  $800^\circ\text{C}$  and could be costed with the same level of confidence as the  $760^\circ\text{C}$  application.

Table 4-1 summarizes the assumed construction of both types of heat exchangers used for the calculation as a function of salt inlet temperature. Assumed air inlet temperature is also given for the three salt temperatures that were run. Table 4-2 summarizes the component costs for the  $760^\circ\text{C}$  DCHX with internal insulation. These are installed costs for large storage vessels. Costs for smaller units, such as a  $1 \times 1$  m DCHX, would be greater for field erection, but if the units could be fabricated in a shop, the costs given in Table 4-2 would probably be conservative.

#### 4.4 EFFECT OF PACKING SIZE AND TYPE

We need to relate the experimentally measured, heat-transfer coefficients (Section 3.0) to those expected at full-scale. The experimentally measured, heat-transfer coefficients were for a pilot-scale experiment with 0.5-in. stainless Raschig rings, 0.6-in. stainless Pall rings, and a  $350^\circ\text{C}$  salt inlet temperature. The economic calculations assumed 2-in. stainless Pall rings or 2-in. ceramic Intalox saddles and salt inlet temperatures of  $360^\circ$ ,  $560^\circ$ , or  $760^\circ\text{C}$ .

Table 4-1. Materials of Construction

Salt Inlet Temperatures		Direct-Contact Heat Exchanger	Finned-Tube Heat Exchanger
Salt In	Air In		
360°C	200°C	Stainless steel Pall rings in an externally insulated, carbon steel column	Carbon steel tubes and fins
560°C	250°C	Stainless steel Pall rings in an externally insulated, stainless steel column	Stainless steel tubes and fins
760°C	550°C	99% alumina saddles in an internally insulated, carbon steel column with Inconel liner	Incoloy 800 tubes and fins

The pressure drop characteristics of all these packings are well understood. Since the viscosity of molten salt (1.5-3.9 cp) does not differ greatly from that of water (1 cp), using the generalized pressure drop correlating Figure 3-4 with appropriate property values for salt should be adequate for pressure drop calculations for any packing.

Heat-transfer performance, however, is not well characterized. Even if one wishes to use mass-transfer data, results will be restricted to 1-in. or 2-in. Raschig rings or Berl saddles. As mentioned in Section 2.0, we had to

Table 4-2. Installed Materials Cost, 760°C DCHX

Component	Material	Cost 1981\$
Packing	99% alumina saddles	\$2489/m <sup>3</sup>
Liner	Inconel	\$283/m <sup>2</sup>
Firebrick	Krilite 30	\$809/m <sup>3</sup>
Column	Carbon steel	(Eq. 4-4b)
Insulation, outer	Glass fiber	\$265/m <sup>3</sup>
Lagging	Aluminum	\$25/m <sup>2</sup>

extrapolate down to 0.5-in. Raschig rings to calculate expected heat-transfer coefficients for the experiment from mass-transfer data. For the 2-in. Pall rings or 2-in. Intalox saddles used in the economic calculations, no information is available either in the form of mass-transfer or heat-transfer data. Therefore, we must comment on the applicability of 0.5-in. Raschig ring heat-transfer data (Section 3.0) to the 2-in. Pall ring or 2-in. Intalox saddle data used in the economic calculation and 0.6-in. Pall ring data.

For a given packing type, increasing the size reduces the pressure drop at fixed G and L because the column flow area is less restricted. For fixed G and L, however, the mass-transfer coefficient is reduced for a larger packing, presumably because the larger packing cannot provide as much interfacial surface area between the gas and the liquid. However, the higher flow capacity of the larger packing offsets this, and the maximum mass-transfer coefficient (which occurs near column loading) is only weakly dependent on packing size. This is illustrated in Figure 4-2 where mass-transfer and pressure-drop data from Norton Chemical (1977) on metal Raschig rings 0.6 in., 1 in., 1.5 in., and 2 in. in size were superimposed on one plot. The maximum mass-transfer coefficient for the 2-in. rings is about 75% of the maximum for the 0.6-in. rings. The four points are the mass-transfer coefficients for DCHX operation at a pressure drop of 0.5-in. of water per foot. With this comparison, the largest rings again have a mass-transfer coefficient about 75% that of the

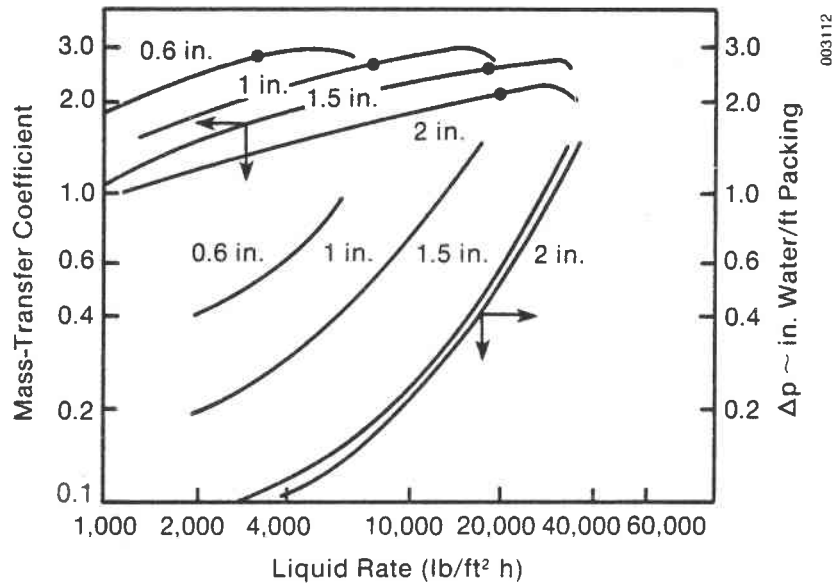


Figure 4-2. Mass-Transfer Coefficient for Various Sizes of Raschig Rings

# Air Molten Salt Direct-Contact Heat Exchange<sup>1</sup>

M. S. Bohn

Solar Energy Research  
Institute,  
1617 Cole Boulevard,  
Golden, Colo. 80401

*Volumetric heat transfer coefficients for direct-contact heat exchange between air and molten nitrate salt have been measured as a function of air and salt flow rates at 350°C salt inlet temperature. Using these heat transfer data for a packed column-type heat exchanger, an economic analysis was used to compare direct-contact heat exchange with conventional finned-tube heat exchangers. High volumetric rates of heat transfer (2000–3000 W/m<sup>3</sup> °C) and flexibility in choice of materials of construction allow one to realize significant economic benefits by using direct-contact heat exchange in this application.*

## Introduction

Direct-contact heat transfer is the transfer of heat across the phase boundary of two immiscible fluids including two liquids, or a liquid and a gas. Conventional heat exchange technology involves the transfer across a solid boundary such as the wall of a steel tube in a shell-and-tube exchanger or across a plate in plate heat exchangers. In the case where the two fluids do not react and can be separated after the heat exchange has been affected, direct-contact heat exchange (DCHX) has several advantages over conventional heat exchangers. Without the intervening wall, a lower thermal resistance is present, and fouling of the heat exchange surface is not a problem. Intimate mixing of the two fluid streams can produce very high rates of heat transfer. The heat exchanger design can be simpler, require less materials of construction, and provide more flexibility in choice of materials.

The DCHX consists of a column substantially filled with a packing material. The packing material consists of rings or saddles that are generally 5 to 7.5 cm in size for large columns and are dumped in the column in a random arrangement. The denser fluid is introduced at the top of the vessel and flows downward; the other is introduced at the bottom of the vessel and flows countercurrently up through the vessel. By properly distributing the liquid at the top of the packing, the flow occurs in the form of many small rivulets flowing over the packing. The packing increases the surface area between the two phases and increases the time during which the liquid stream is exposed to the gas, greatly increasing the rate of heat transfer per unit volume of heat exchanger.

Direct-contact heat exchange is especially attractive in applications in which it is necessary to transfer heat between a gas and a liquid because high rates of heat transfer can be achieved without the added expense of finned tubes. Among solar thermal technologies, two examples include high-temperature process air and the Brayton cycle (Fig. 1). In both examples, solar energy provides a heat source at a central

receiver in which molten salt cools the receiver, and transfers the solar energy to a storage device. Molten salt is the logical heat transfer fluid at high temperatures because it exhibits low-vapor pressure, high sensible heat storage, excellent heat transfer characteristics, and because it is relatively benign toward receiver containment materials (at temperatures below 600°C for state-of-the-art salts).

In either concept, it is necessary to transfer heat from the molten salt to air. Conventional heat-exchange technology for transferring this heat would be a finned-tube heat exchanger. The molten salt is pumped through the tubes and air is pumped over the finned outside surface of the tubes. In the DCHX concept, molten salt would be introduced at the top of a packed column and the air would be blown up through the bottom of the column.

Because of the lack of heat transfer data or design correlations, it is not possible at this time to accurately assess the economic potential of direct-contact heat exchange. Such an assessment requires us to determine the rate of heat transfer per unit volume in the DCHX. This determines the required size (and therefore cost) of the column needed to deliver the required amount of heat to the air. It also determines the costs associated with operating the equipment—primarily, the cost of blowing the air through the column. It is possible to use mass transfer data to estimate heat transfer rates by assuming that the mass transfer-heat transfer analogy is valid [1]. However, an experimental determination of the heat transfer coefficients is advisable before proceeding with detailed economic studies.

The purpose of the present work is threefold: (i) the experimental determination of heat-transfer coefficients in direct-contact heat exchange between molten salt and air, (ii) the calculation of these heat-transfer coefficients based on the mass transfer analogy and comparison with the experimental data, and (iii) an economic analysis using the experimental data and comparing DCHX with conventional finned-tube heat exchangers. In general, the objective of the present work is to determine if, and in what applications, DCHX is a cost-effective technology. This paper describes the experimental apparatus, methods, and the results that are compared with the calculated values. Then, results of an economic analysis

<sup>1</sup>Prepared for the U.S. Department of Energy, Contract No. DE-AC02-83CH10093.

Contributed by the Solar Energy Division for publication in the JOURNAL OF SOLAR ENERGY ENGINEERING. Manuscript received by the Solar Energy Division, April, 1984.

increase bubble rise time

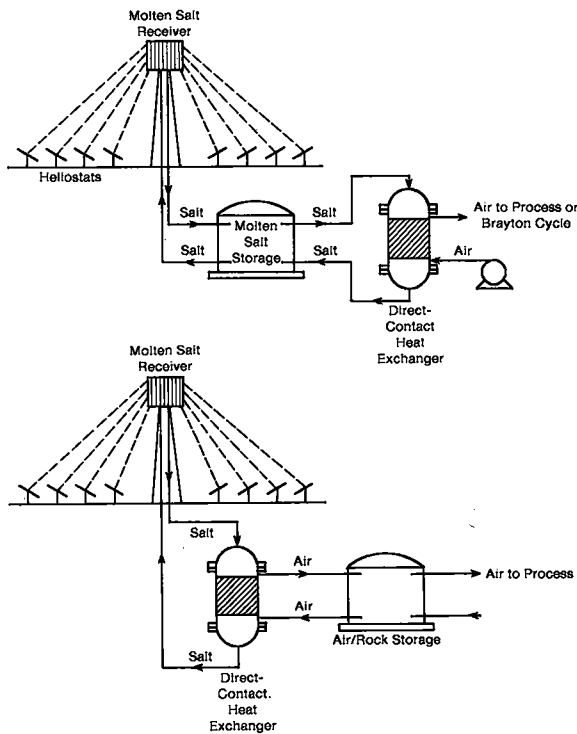


Fig. 1 Applications for direct-contact heat exchangers in solar energy

are presented that compare the cost-effectiveness of DCHX and finned-tube heat exchangers in several applications.

### Experimental Measurements of Volumetric Heat Transfer Coefficients

**Description of the Apparatus.** A flow diagram of the experimental apparatus is given in Fig. 2, and a detailed diagram of the packed column is shown in Fig. 3. The test loop is operated in a batch mode, with regulated air pressure on the upper tank providing regulated salt flow through the salt valve. The upper tank is filled with molten salt and pressurized to approximately 50 kPa gauge. In this way, the salt flow is affected minimally by the loss of salt head in the upper tank. The salt flows through the salt valve into the top of the column and into a distributor that provides uniform salt flow in the bed. The packed bed is supported by a gas injection support plate that allows the salt to flow downward while providing a uniform air distribution at the bottom of the packing. After the air passes up through the bed, it flows around the annular gap between the salt distributor and the inside diameter of the column. The air then flows through a wire mesh mist eliminator that removes small salt droplets before the air flows out of the column. Salt flowing out of the bottom of the bed is returned to the lower salt tank. The entire test loop, with the exception of the salt valve, was constructed of 304 stainless steel. The salt valve was constructed of 316 stainless steel.

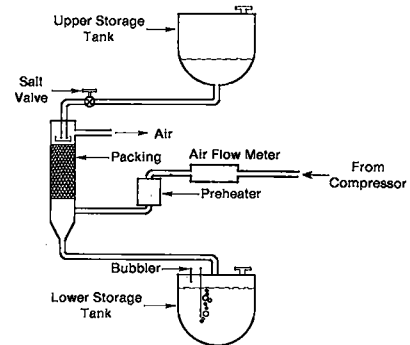


Fig. 2 Flow diagram of a direct-contact heat exchanger test loop

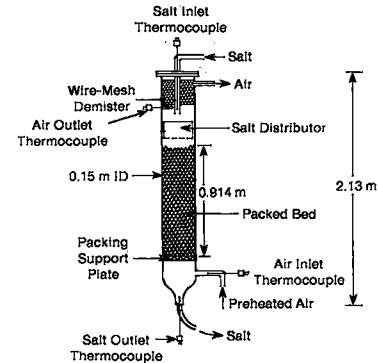


Fig. 3 Details of the packed column used in present study

A maximum operating temperature of 350°C was chosen because common nitrate salts do not cause excessive corrosion with stainless steel alloys at or below that temperature. A commercial heat-treating salt, which is a mixture of potassium nitrate, sodium nitrate, and sodium nitrite and melts in the range from 150° to 200°C, was used for the tests. Electrical heat tracing was used to bring the loop initially up to operating temperature and to maintain this temperature. The tracing consisted of a stainless shell with nichrome wire inside, insulated from the shell with a refractory insulation. Approximately 50 m of the heat tracing was required to provide adequate heating. The test loop was then insulated with ceramic wool blanket to a thickness of approximately 15 cm. Air supplied at the bottom of the column was preheated by a 9-kW electric preheated power by an SCR (silicon-controlled rectifier) power supply. A proportional-integral process controller supplied the control signal to the SCR power supply based on the desired air temperature and the measured air temperature at the preheater outlet. A two-cylinder, oil-free, 7.5 kW compressor supplied air to the preheater.

Two types of commercial column packing were tested. Most data were for 1.27-cm stainless steel Raschig rings which are essentially 1.27-cm-long sections cut out of 1.27-cm o.d., 0.16-cm wall stainless tubing. The second type of packing tested was 1.59-cm stainless steel Pall rings which are similar

### Nomenclature

$a$ = surface area per unit volume ( $m^{-1}$ )	$\dot{m}_s$ = salt flow rate (kg/hr)	$Ua$ = overall volumetric heat transfer coefficient ( $W/m^3 \text{ } ^\circ C$ )
$c_p$ = air specific heat ( $J/kg \text{ } ^\circ C$ )	$Q_a$ = rate of heat transfer to the air (W)	$U$ = overall heat transfer coefficient ( $W/m^2 \text{ } ^\circ C$ )
$c_s$ = salt specific heat, liquid ( $J/kg \text{ } ^\circ C$ )	$Q_s$ = rate of heat transfer from the salt (W)	$V_p$ = volume of packing ( $m^3$ )
$G$ = gas loading ( $kg/hr \text{ } m^2$ )	$T_{ai}$ = air inlet temperature ( $^\circ C$ )	$\Delta T_m$ = log mean temperature difference ( $^\circ C$ )
$L$ = liquid loading ( $kg/hr \text{ } m^2$ )	$T_{ao}$ = air outlet temperature ( $^\circ C$ )	
$\dot{m}_a$ = air flow rate (kg/hr)	$T_{si}$ = salt inlet temperature ( $^\circ C$ )	
	$T_{so}$ = salt outlet temperature ( $^\circ C$ )	

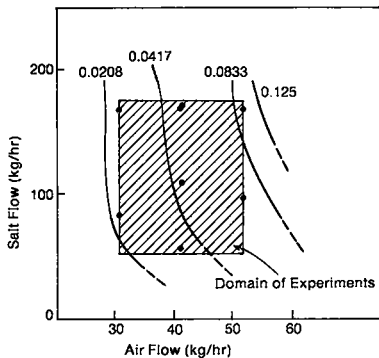


Fig. 4 Column operating map and experimental conditions. Parameter on curves is column pressure drop in cm water column per cm bed height. • = location of operating conditions tested.

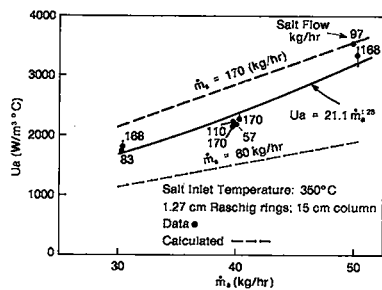


Fig. 5 Overall volumetric heat transfer coefficients and comparison with values calculated from the mass transfer analogy

to the Raschig rings except that several "spokes" have been punched in from the ring periphery toward the axis to provide more flow area. While the Pall rings provide a similar surface area per unit volume as the Raschig rings, the openings in Pall rings provide freer flow path for the air and thus operate with a lower air-side pressure drop.

**Instrumentation.** The air flow rate was measured by an inline mass flow transducer calibrated to  $\pm 2$  percent of reading by the manufacturer, Datametrix, Inc. The salt flow rate was determined by a bubbler system which continuously monitored the level of salt in the lower salt tank. The lower tank volume was calibrated before the tests by filling it with water in 5-liter increments and recording the bubbler voltage output.

All thermocouples were Chromel-Alumel (type K). Salt inlet temperature was determined by a probe inserted into the vertical portion of the pipe from the upper tank. This probe should be a very good measure of salt inlet temperature since it was totally immersed in salt just before it flowed into the salt distributor. This temperature was typically within  $2^\circ\text{C}$  of the upper-tank salt temperature. Salt outlet temperature was determined by a probe inserted in the pipe leading out of the bottom of the column. The probe was inserted just to the point where the cone at the bottom of the column begins to expand. The probe was exposed to rivulets dripping from the packing support plate and was the best compromise for measuring salt outlet temperature. Constraints on this measurement include the trace heating on the column wall, which could affect the temperature of salt flowing along the wall, and air entering the column at a lower temperature than the salt leaving the column, which could reduce the outlet salt temperature reading if the probe were inserted further into the column. The response of this probe to sudden changes in the salt flow, air flow, and air inlet temperature suggested that the probe gave a good indication of salt outlet temperature. Air inlet temperature was determined by a probe inserted into the horizontal portion of the air inlet pipe and sensed the temperature of the air about 20 cm from the column. Air outlet temperature was determined by a probe inserted through the

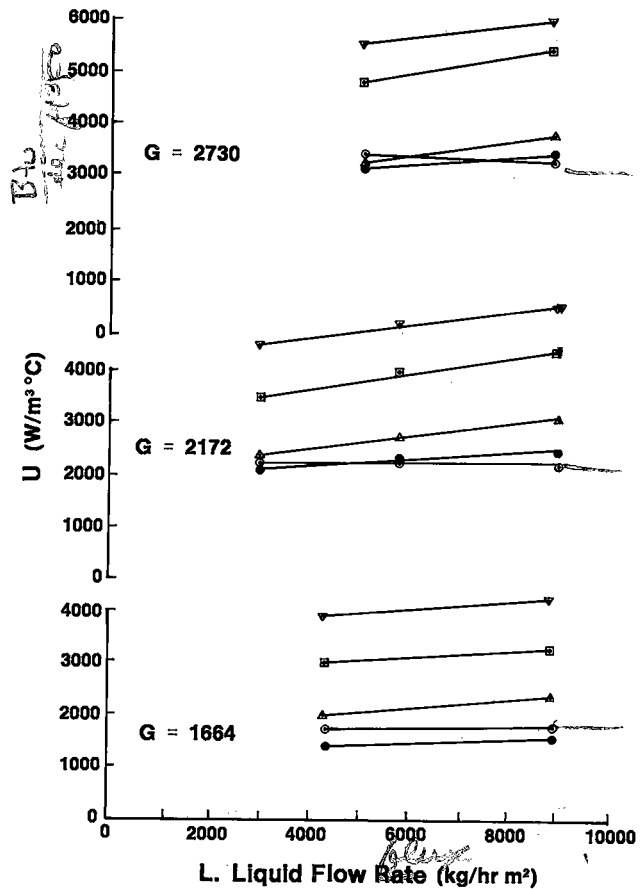


Fig. 6 Comparison of recent direct contact heat transfer data.  $G$  = gas flow rate,  $\text{kg/hr m}^2$ .  $\odot$  Present work, 1/2 in. Raschig rings (RR), air-molten salt;  $\bullet$  Hujtsak [3], 1/2 in. RR, air-oil;  $\triangle$  Pohlentz [4], 1 in. RR, air-oil;  $\square$  Yoshida [5], 15-35 mm RR, air-water;  $\nabla$  McAdams et al. [6], 1 in. RR, air-water.

column just below the mist eliminator. Secondary measurements included upper-tank salt and surface temperatures, lower-tank surface temperature, column surface temperature, bed temperature, and the pressure differential between the preheater outlet pipe and the column air outlet pipe.

Data were recorded by a Hewlett Packard Model 85 microcomputer that gave printed, displayed, and plotted information. A Leeds and Northrup strip chart also recorded surface temperatures, air flow rate, and bubbler output.

**Heat Transfer Measurements and Procedures.** Using the inlet and outlet salt and air temperatures and the salt and air flow rates, the rate of heat transfer can be determined from

$$Q_s = \dot{m}_s c_s (T_{si} - T_{so}) \quad (1)$$

$$Q_a = \dot{m}_a c_p (T_{ao} - T_{ai}) \quad (2)$$

Equation (1) gives the rate of heat transfer from the salt and equation (2) gives the rate of heat transfer to the air. A comparison of  $Q_s$  and  $Q_a$  gives a quantitative measure of the quality of the heat transfer data since, in the absence of heat losses and measurement errors,  $Q_a = Q_s$ . Therefore, the absolute value of the quantity  $100(1 - Q_s/Q_a)$  percent could be called the heat balance parameter for the experiment.

Following Fair [1], the volumetric heat transfer coefficient can then be calculated from

$$Ua = \frac{Q}{V_p \Delta T_m} \quad (3)$$

where  $V_p$  is the volume of the packing ( $0.0167 \text{ m}^3$ ) and  $\Delta T_m$  is the log-mean temperature difference:

**Table 1 Heat transfer data and comparison with mass transfer calculations**

Salt inlet temperature ( $T_{si}$ ), (°C)	Air flow ( $\dot{m}_a$ ), (kg/hr)	Salt flow ( $\dot{m}_s$ ), (kg/hr)	Measured $Ua$ ( $W/m^3 \text{ } ^\circ C$ )	Heat balance parameter	Calculated $Ua$ ( $W/m^3 \text{ } ^\circ C$ )
330	30.8	130	1595	$\pm 0.5\%$	- <sup>a</sup>
342	30.8	168	1820	3	2171
348	30.9	83	1771	2	1429
330	39.6	126	2404	7	- <sup>a</sup>
341	40.7	171	2252	6	2896
353	40.5	57	2203	3	1478
349	40.3	170	2164	4	2854
348	40.2	110	2228	1	2189
348	50.5	96	3520	5	2535
330	50.7	138	2829	5	- <sup>a</sup>
342	50.9	168	3351	5	3574

<sup>a</sup>Pall ring.

$$\Delta T_m = \frac{(T_{si} - T_{ao}) - (T_{so} - T_{ai})}{\ln\left\{\frac{T_{si} - T_{ao}}{T_{so} - T_{ai}}\right\}} \quad (4)$$

The value of  $Q$  in equation (3) can be either  $Q_s$  or  $Q_a$ . The heat balance parameter directly measures the error in reported  $Ua$ .

Experimentally, it was possible to vary the salt flow rate, the air flow rate, and the salt and air inlet temperatures. The last two variables are of secondary importance (as long as the air inlet temperature is above the salt freezing point) and were, therefore, not varied in any systematic way. The salt flow rate was varied from 50 to 170 kg/hr and the air flow was varied from 30 to 50 kg/hr. Higher salt flow rates could be attained, but this would have resulted in run times too short to establish steady conditions—a crucial requirement for good data as indicated by small values of the heat balance parameter. Air flow rates much larger than 50 kg/hr would produce column flooding. As shown in Fig. 4, the operating conditions tested adequately covered the operating map for the column. The contour labeled 0.125 corresponds to the loading line (the line beyond which pressure drop increases very rapidly) for this packing. The contour through the center of the data labeled 0.0417 corresponds to a typical packed column operating pressure drop (1/2 in. water column per foot of bed height in English units).

The system was maintained at operating temperature continuously for about six months, with the exception of downtime for repairs. To minimize the time required to reach steady state, the heat trace was set so that the bed temperature was fairly close to the upper-tank salt temperature. Pressure was applied to the upper tank from the regulated air supply and the salt valve was opened. Achieving constant salt flow rate, as indicated by the bubbler output trace, generally required 20 minutes. Air flow could then be set to the desired value, and when steady state was achieved and data were recorded, the air flow could be adjusted to a new setting. An examination of the data indicated that the best heat balances were achieved when the salt flow was uniform and when no adjustments of the salt valve or tank pressure were necessary during the run.

Salt carryover was not measured. As shown in Fig. 3, the only precaution against loss of entrained salt droplets was a wire-mesh mist eliminator. Several hours of testing with a knockout pot attached to the air outlet port did not reveal any substantial accumulation of salt; however, commercial operation will require continuous operation and accumulation of salt in piping or process equipment, or impingement of salt particles on turbine blades will be intolerable. Therefore, a more detailed study of carryover rates is necessary. Also needed is a more detailed study of the degradation of various heat transfer salts due to contact with air.

**Results and Discussion.** Experimental data are presented in Fig. 5 in the form of volumetric heat transfer coefficient versus air flow rate with salt flow as a parameter, in addition to calculated values based on the mass transfer analogy [1]. The data are also shown in Table 1, with heat transfer coefficients calculated from the mass transfer analogy [1]. Only the Raschig ring data are shown in Fig. 5.

The experimental heat transfer coefficients do not appear to depend on salt flow rate; note that all the data for  $\dot{m}_a = 40$  kg/hr and for  $57 \leq \dot{m}_s \leq 170$  kg/hr vary by only a few percentage points. The variation with air flow is relatively strong—a best fit produces

$$Ua = 21.1 \dot{m}_a^{1.28}, \quad (5)$$

where  $\dot{m}_a$  is in kg/hr and  $Ua$  is in  $W/m^3 \text{ } ^\circ C$ .

These data are compared with similar volumetric heat transfer measurements by Hujak [3], Pohlentz [4], Yoshida [5], and McAdams et al. [6], in Fig. 6. The data are plotted for the three gas loadings used in the present study. The data appear to fall into two groups—one group for air-water systems and another group for air-oil systems. The air-water group exhibits consistently higher volumetric heat transfer probably due to heat transfer by evaporation of water compared to pure sensible heat transfer for the air-oil systems. The present data for air-molten salt, which is also a pure sensible heat transfer system, compares very favorably with the air-oil systems. One difference which may be seen in Fig. 6 is that while the air-molten salt system exhibit no measurable sensitivity to liquid flow rate, the air-oil systems do exhibit a weak sensitivity. This could be related to better wetting of the packing by the salt compared to oil. If the salt wets the packing completely, one would not expect that increasing liquid flow rate would make more heat transfer surface available. Since the present data compare favorably with previous air-oil data it would appear that heat transfer mechanisms do not differ greatly for the systems. At higher temperatures however, the air-molten salt system will be affected by radiation heat transfer resulting in thermal backmixing thereby reducing the heat exchange effectiveness. Further data and analysis at higher temperatures are required.

Heat transfer data for the Pall rings were taken at 130 kg/hr salt flow for air flow of 30, 40, and 50 kg/hr (see Table 1). The values of  $Ua$  did not vary significantly from the correlation line, equation (5). However, the pressure drop for Pall rings is much less than that of the Raschig rings at a given air flow as expected. Therefore, one would expect that at a given pressure drop, the Pall rings would give significantly higher heat transfer since a higher air flow would be required.

As shown in the last column of Table 1 as well as in Fig. 5, heat transfer coefficients calculated by Fair's method [1] from mass transfer data underestimate measured heat transfer coefficients, except at large salt flows. As discussed by Huang [7], mass-transfer correlations generally underpredict heat

transfer due to conduction of heat in the packing. Mass transfer has no analogy to conduction heat transfer. Overall heat transfer coefficients calculated from mass transfer data are shown in Fig. 5 for two salt flow rates, 170 and 60 kg/hr. These results further demonstrate the lack of sensitivity to salt flow rate of the heat transfer data compared with that predicted from the mass transfer data, and that some caution is required in applying the mass transfer-heat transfer analogy.

### Economic Analysis

With experimental values for the heat transfer coefficient, one can proceed to determine the economic value of DCHX. Rather than basing economic calculations solely on the mass transfer data, actual heat transfer data should give us more confidence in the results. For several reasons, the experimental data cannot be applied directly to a commercial-size DCHX; therefore, even these results require some caution in interpretation.

**Method of the Analysis.** An economic comparison of DCHX and finned-tube exchangers can be made by considering all capital and operating costs associated with the heat exchanger. The methodology then calculates the annual levelized cost [2]. The annual levelized cost is the constant annual cost (in fixed 1981 dollars) which, if paid over the lifetime of the heat exchanger, would have a present value equal to the present value of the actual costs incurred over the lifetime of the heat exchanger. The economic parameters assumed the following values: discount rate = 10 percent, general inflation rate = 6 percent, operating and maintenance costs escalation = 6 percent, fuel cost escalation = 8 percent, first year of commercial operation = 1990, and effective corporate income tax rate = 50 percent.

To determine capital cost, we must know the size of the heat exchanger and the materials of construction. The first is determined by the required heavy duty, overall heat-exchange coefficients, and log-mean temperature differences. Materials of construction are determined by operating temperature and working fluids. For the sake of consistency, all capital costs have been determined from data given by reference [8] for finned-tube heat exchangers and for packed columns.

For the finned-tube heat exchanger, we used the characteristics of the heat exchanger core denoted CF8.8 1.0J (A) by reference [9], which consists of 2.54-cm o.d. tubes on 4.98-cm spacing with spiral-wound fins—at 3.5 fins per cm and 0.031-cm fin thickness. In this arrangement salt flows through the tubes and air flows across the finned-tube banks (crossflow arrangement). Data on the core include the Colburn-*j* factor (the heat transfer coefficient on the air side) and the friction factor as a function of air-side Reynolds number. The salt-side Reynolds number was designated a constant (10,000) because the overall heat transfer coefficient was not a strong function of the salt-side Reynolds number as long as the salt flow was turbulent. Also, salt-side pumping work is negligible, so salt-side pressure drop need be considered only from the standpoint of tube stress at elevated temperatures. In an attempt to provide the finned-tube heat exchanger with more air-side surface, the heat exchanger core, CF8.0-1/8T was also used in the calculation. This core has smaller tubes and more densely packed fins. Results of the calculation showed that excessive air-side pressure drop resulted and that this core was less cost-effective than CF8.8 1.0J.

Given the flow rates (determined from the given heat duty and terminal temperatures) and the terminal temperatures, the heat exchanger effectiveness is determined. Then, the required number of transfer units (NTU) is determined from equations for crossflow heat exchangers. Beginning with the lowest air-side Reynolds number for which the heat exchanger core data are given, the frontal area of the core is determined,

the air-side heat transfer coefficient is calculated, the fin efficiencies are calculated, and the overall heat transfer coefficient is then determined. From NTU one may calculate the total heat transfer surface required which determines the core dimension in the air flow direction and the core pressure drop. After the surface area and pressure drop are obtained, the annual levelized cost may be calculated. This procedure is repeated for increasing air-side Reynolds numbers until the minimum annual levelized cost is found. The heat exchanger core was restricted to the maximum heat transfer area for which cost data are presented in reference [8]; 900 m<sup>2</sup>. This corresponds to a shell diameter of 2.77 m for 4.87-m-long, 2.54-cm-o.d. tubes. Multiple heat exchangers are specified when heat duties require more than this maximum heat transfer area.

Optimization of the DCHX is somewhat different because of flooding constraints. Outlet air temperature cannot be specified a priori. Beginning with a column diameter of 1 m (the smallest diameter for which cost data are available), the volume of packing is calculated. (The shortest practical column height, equal to the diameter, was used because this always minimized annual cost. Column diameters much larger than the column height produce problems with uniform salt and air distribution in the column.) For an assumed value of the overall heat-transfer coefficient, the log-mean temperature is determined, and, therefore, the air outlet temperature is known. This determines the air flow rate; from the generalized pressure drop correlation available for most common column packings, we may determine the pressure drop. Column diameters that produce operating conditions off the generalized pressure drop map are rejected. A maximum column diameter of 5 m was used, since this is the largest for which reference [8] gives cost data. The packing type used in the calculations was 5-cm stainless steel pall rings. With the column size and pressure drop, the annual levelized cost may be calculated. The procedure is repeated for increasing column diameters, giving annual cost as a function of approach temperature (air outlet temperature). The overall volumetric heat transfer is taken as a parameter; the values  $Ua = 2000, 3000, \text{ and } 4000 \text{ W/m}^3 \text{ } ^\circ\text{C}$  were used. We can then use the experimental values of  $Ua$ , or the calculated values of  $Ua$ , along with the results of this economic calculation (which will give sensitivity to  $Ua$ ) to appraise the economic viability of DCHX relative to finned-tube heat exchangers.

From exposure tests of up to 4500 hours at temperatures up to about 600°C, reference [10] demonstrates that stainless steel alloy 316 will oxidize at the rate of 5 mil/yr or less, typically 2 mil/yr. A 90-mil tube wall thickness should therefore be adequate for a 20-year life. Fin material will also have to be stainless steel due to manufacturing constraints and materials compatibility considerations. For the packed column at 600°C or lower, we specify stainless Pall rings for the packing, and a stainless steel column with external insulation. Internal insulation with a liner to contain the salt and support the load due to the packing would allow the use of a carbon-steel column, greatly reducing the cost. This insulation method has been tested [11], but is not commercially available at this time. It therefore represents some technical risk.

At temperatures above 600°C, common nitrate heat transfer salts decompose. Research is ongoing to identify candidate heat transfer salts and compatible containment materials for temperatures above 600°C. Based on state-of-the-art knowledge it would appear that Incoloy 800 alloy would be a reasonable material choice for finned-tube heat exchange materials for temperatures up to 800°C.

For temperatures up to 800°C, the DCHX consists of an internally insulated, carbon-steel column similar in design to the storage tank described in reference [11]. A high purity (99

total cost!

the tank  
properly cost reduction



1 kWh = 3.6 x 10<sup>6</sup> J

1 GJ = 277 kWh

**Table 2 Materials of construction**

Temperatures		DCHX	Finned-tube
Salt in	Air in		
360°C	200°C	Stainless Pall rings in an externally insulated carbon-steel column	Carbon-steel tubes and fins
560°C	250°C	Stainless Pall rings in an externally insulated stainless steel column	Stainless tubes and fins
760°C	550°C	99 percent alumina saddles in an internally insulated carbon-steel column with Inconel liner	Incoloy 800 tubes and fins

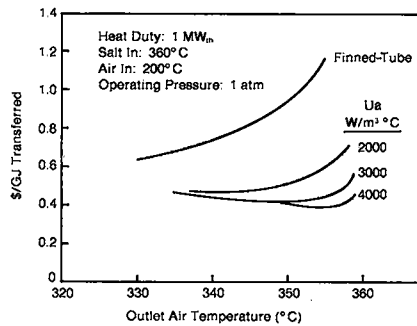


**Fig. 7 Cost comparison for 360°C, 1 atm, 1 MW<sub>th</sub>**

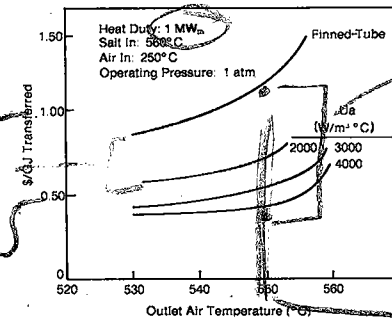


**Fig. 8 Cost comparison for 560°C, 1 atm, 1 MW<sub>th</sub>**

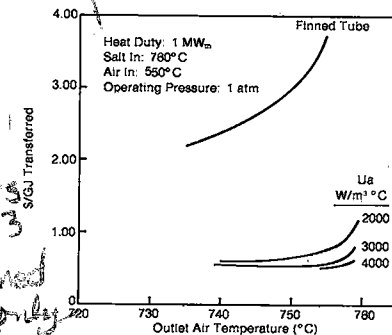


**Fig. 9 Cost comparison for 760°C, 1 atm, 1 MW<sub>th</sub>**

percent alumina) packing will be required to resist attack by the salt. To seal the insulating firebrick from the salt, an Inconel liner will be required. A layer of glass fiber insulation will cover the outside of the column and aluminum lagging will weatherproof the assembly.

High-purity alumina packing is not commonly available. The cost of this packing was determined from the cost ratio (3:1) between 99 percent and 57 percent alumina catalyst support from Norton Chemical Company. To account for unknown manufacturing difficulties that could arise when fabricating saddles from the 99 percent alumina, a very conservative cost factor of 4x was applied to the current price (\$700 per m<sup>3</sup>, 2.8 m<sup>3</sup> order for second quarter 1983 costs) quoted by Norton Chemical Company, giving an equivalent 1981 cost of \$2489/m<sup>3</sup>. This alumina packing is the major cost item for the DCHX, suggesting that it would be worthwhile to investigate more closely the actual cost to manufacture the packing. In the event the foregoing cost estimate proves to be reasonable, the high cost of the packing would lead one to consider a spray column DCHX for the high-temperature applications.

The column liner cost was taken from reference [11] in which an Incoloy liner with a waffled design to accommodate thermal cycling was costed. Since the DCHX will not operate in a cycling mode, the liner can be a simpler design with allowance for thermal expansion. Allowing a 2x cost factor between Incoloy and Inconel [8] and a 1/2x factor for a simpler liner design, the cost of the installed liner is \$283/m<sup>2</sup> of internal column area.

Sufficient thickness of firebrick (Krilite 30) is specified to allow operation of the carbon-steel column below 316°C for an internal temperature of 760°C and to keep thermal losses less than 1 percent of the transferred heat. Cost of the firebrick is \$809/m<sup>3</sup> [11].

The cost of the carbon-steel shell is calculated from data in reference [8]. For the fiberglass outer insulation (sufficient thickness to keep losses to 1 percent of the transferred heat when the ambient temperature is 20°C and the carbon-steel column is 316°C), reference [6] used \$265/m<sup>3</sup> of insulation and \$25/m<sup>2</sup> of aluminum lagging.

Temperatures above 800°C will most likely require ceramic tube-fin heat exchangers. Although the cost of these ceramic heat exchanger tubes is not prohibitive (most likely less than the cost of high alloy tubes), fabrication of the tubes into a

heat exchanger is a relatively unknown art, especially when one considers high-pressure operation and liquid tight seals. Cost projections are therefore difficult. Construction of the packed column, however, would not change drastically for temperature above 800°C and can be costed with the same level of confidence as the 760°C application.

Table 2 summarizes the assumed materials of construction for both types of heat exchangers used for the calculation as a function of salt inlet temperature. The assumed air inlet temperature is also given for the three salt temperatures that were assumed for the analysis.

It will be necessary to perform heat-transfer experiments at full scale to determine how a larger packing required for commercial-size columns performs relative to the 1.2-cm packing tested here before recommending DCHX for commercial application. Based on experimental data and corresponding heat transfer coefficients calculated from mass transfer data, an appropriate range of heat-transfer coefficient  $Ua$  for the 1.2-cm Raschig rings is 1800–3500 W/m<sup>3</sup>·°C. It seems reasonable to perform the economic calculations based on a range of  $Ua$  from 2000–4000 W/m<sup>3</sup>·°C for the commercial-size DCHX. One can then assess the sensitivity of the economics on  $Ua$  until a full range of data at full scale is made available.

**Results.** Figures 7–9 give the results of the economic analysis. Each figure gives the cost of transferring 1 GJ of energy as a function of air outlet temperature. The graphs present results for atmospheric pressure operation. As the air outlet temperature approaches the salt inlet temperature,

550° Am  $U_A = 3000$

Table 3 Cost of transferring heat via DCHX relative to finned-tube heat exchangers

Salt inlet temperature	Operating pressure	
	1 atm	5 atm
360°C	0.44 <sup>a</sup>	0.46
560°C	0.46	0.57
760°C	0.18	0.26

<sup>a</sup>Cost ratio

more surface area for the finned-tube heat exchanger is required and more volume of packing is required for the DCHX. This is because the log-mean temperature difference (equation (4)) is reduced and this increases the packing volume for a fixed heat-transfer coefficient and heat duty (equation (3)). This can be compensated by increasing the air flow to increase the heat-transfer coefficient, but this increases operating costs.

Generally, DCHX provides closer temperature approaches than finned-tube exchangers before a rapid increase in cost results. The curves for the DCHX for given  $U_A$  increase as the temperature approach is decreased for low outlet air temperature because the volumetric heat-transfer coefficient has been artificially fixed, and the only way to reduce outlet temperature is to increase air flow (which drives up the cost). For volumetric heat transfer coefficients as low as  $U_A = 2000 \text{ W/m}^3 \text{ }^\circ\text{C}$ , this effect is generally not seen for the temperature approaches presented, less than 30°C.

Calculations for a higher operating pressure (5 atm, not given in graphical form) were for 5 MW<sub>th</sub> or 2 MW<sub>th</sub> heat duty, while those for 1 atm pressure were for 1 MW<sub>th</sub>. The higher-pressure units generally resulted in maximum-sized packed columns (5 m × 5 m). Larger columns can be built, but since cost data were restricted to a 5-m diameter, calculations were restricted to this diameter for consistency. The finned-tube heat exchanger tended to reach maximum size (900 m<sup>2</sup>) before the DCHX. One major conclusion, then, is that DCHX provides substantially more heat transfer capacity for a given volume of heat exchanger.

The cost advantage of DCHX relative to finned-tube heat exchangers is not a strong function of approach (difference between salt inlet and air outlet temperatures), except for small approaches where the finned-tube costs increase more rapidly. Table 3 gives the cost ratio from all size cases at a 10°C approach. The DCHX data for  $U_A = 3000 \text{ W/m}^3 \text{ }^\circ\text{C}$  were used in each case.

There appears to be no large decrease in this cost ratio in going from 360°C to 560°C, because the cost of construction materials increased substantially for both types of heat exchangers. If we used an internally insulated carbon-steel packed column with stainless steel Pall rings for 560°C, a

significant improvement would result. (Since this represents a larger technical risk than the externally insulated stainless steel column, it is not a fair comparison with commercially available stainless steel finned-tube heat exchangers.) The large reduction in relative cost in going from 560° to 760°C is due to the avoidance of high alloys in the DCHX, while the finned-tube does require such materials of construction. Even though the high-purity alumina packing is more costly than a stainless steel packing, using a carbon-steel column provides a very large cost advantage over the Incoloy finned-tube heat exchanger.

**Conclusions.** Volumetric heat-transfer coefficients in the range of 1800–3500 W/m<sup>3</sup> °C were measured experimentally for a packed-bed air-molten salt direct-contact heat exchanger and agree well with previous data for air-oil systems. The coefficient depends on air flow rate but not on salt flow rate. Heat-transfer coefficients based on mass transfer data show dependence on both air flow and salt flow. Radiation backmixing may decrease the performance of air-molten salt systems operating at higher temperatures and further data and analyses at higher temperature are needed.

The measured heat-transfer coefficients are large enough to imply that direct-contact heat exchangers should be much more cost-effective than conventional finned-tube heat exchangers. At low to mid-temperatures (360°–560°C), the levelized annual cost (capital and operating) ratio should be about one-half; at high temperatures (>600°C), where high-alloy steels will be required in the finned-tube heat exchanger, the cost ratio is about one-fifth. The cost advantage is due to high rates of heat transfer and the ability to use materials other than high alloys to contain the salt.

**References**

- 1 Fair, J. R., "Designing Direct Contact Coolers/Condensers," *Chemical Engineering*, June 1972, pp. 91–100.
- 2 Bohn, M. S., "Air/Molten Salt Direct-Contact Heat Transfer Experiments and Economic Analysis," SERI/TR-252-2015, Golden, Colo., 1983.
- 3 Hujsak, K. L., "The Transfer of Heat Between Air and a Nonvolatile Oil in a Packed Tower," M.S. thesis, Massachusetts Institute of Technology, 1947.
- 4 Pohlentz, J. B., "Heat and Mass Transfer in Packed Towers," Ph.D. thesis, Massachusetts Institute of Technology, 1947.
- 5 Yoshida, F., and Tanaka, T., *Ind. Eng. Chem.*, Vol. 43, No. 6, p. 1467.
- 6 McAdams, W. H., Pohlentz, J. B., St. John, R. C., *Chem. Eng. Prog.*, Vol. 45, No. 4, 1949, p. 241.
- 7 Huang, C., "Heat Transfer by Direct Gas-Liquid Contacting," M.S. thesis, University of Texas at Austin, May 1982.
- 8 Peters, M., and Timmerhaus, K., *Plant Design and Economics for Chemical Engineers*, 3rd ed., McGraw-Hill, New York, 1980.
- 9 Kays, W. M., and London, A. L., *Compact Heat Exchangers*, McGraw-Hill, New York, 1964.
- 10 Tortorelli, P. F., and DeVan, J. H., "Thermal Convection Loop Study of the Corrosion of Fe-Ni-Cr Alloys by Molten NaNO<sub>3</sub>-KNO<sub>3</sub>," ORNL/TM-8298, Oak Ridge National Laboratory, Oak Ridge, Tenn., 1982.
- 11 Martin Marietta, "Internally Insulated Thermal Storage System Development Program," MCR-79-1369, Martin Marietta Aerospace Corp., Denver, Colo., 1979.

both  
 Looks like LEC for 600°C  
 HXERS are in the noise (±5%)  
 compared to rest of power plant?  
 Compare to cost of producing thermal  
 energy which is usually much lower.  
 if  $\eta_{TE} = .33$ , LEC is  $1/3$   
 for thermal over elec.  
 Transactions of the ASME  
 on annual basis

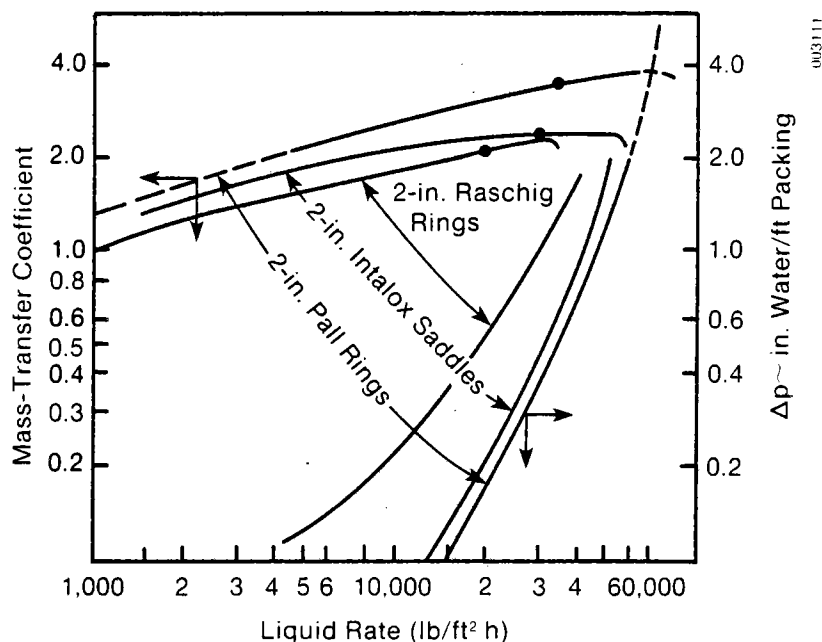


Figure 4-3. Mass-Transfer Coefficient for Various Types of Packing

0.6-in. rings (mass-transfer data for 0.5-in. Raschig rings was not available). It appears that heat-transfer coefficients for 2-in. Raschig rings should be about 75% of that measured in the present column at a given pressure drop.

Comparing the measured heat-transfer coefficients with calculated values based on mass transfer (see Figure 3-6), we found that the mechanisms of heat transfer and mass transfer appear to differ and that the mass-transfer/heat-transfer analogy does not apply. We have some experimental evidence (Figure 3-7) suggesting that heat transfer does not depend on packing type, at least when changing from Raschig rings to Pall rings. Figure 4-3 depicts the effect of packing type on mass transfer. However, since the analogy with heat transfer is suspect, we must assume that the 2-in. Pall ring (as used in the economic calculations) transfers the same amount of heat as the 0.5-in. Raschig ring at a given air mass velocity  $G$ . Pressure-drop performance for the 2-in. Pall rings is accounted for in the calculation procedure, so the reduced pressure drop caused by the Pall rings is taken into account.

Based on the experimental data presented in Section 3.0, an appropriate range of heat-transfer coefficient  $Ua$  for the 0.5-in. Raschig rings and therefore the 2-in. Pall rings is  $1800\text{--}3500\text{ W/m}^3\text{ }^\circ\text{C}$ . From the previous discussion it is reasonable to perform the economic calculations based on a range of  $Ua$  from  $2000\text{--}4000\text{ W/m}^3\text{ }^\circ\text{C}$ . We can then assess the sensitivity of the economics on  $Ua$  until a full range of data at full scale is made available.

#### 4.5 RESULTS

Figures 4-4 through 4-9 present the results of the economic analysis. Each figure shows the cost of transferring 1 GJ of energy as a function of air-outlet temperature. For each temperature range two graphs give results for 1 atm and 5 atm operating pressure. The 1 atm case represents process-heat applications, and the 5 atm case represents a Brayton-cycle application. The Brayton cycle probably will not apply to the two lower temperatures, but higher pressure operation is generally more economical because of increases in air density, and, therefore, the low-temperature, high-pressure case may have application in process heat.

As the air-outlet temperature approaches the salt-inlet temperature, the finned-tube heat exchanger needs a larger surface area and the DCHX requires more packing. This is because the log-mean temperature difference (Eq. 3-4) is reduced, and this increases the packing volume for a fixed, heat-transfer coefficient and heat duty (Eq. 3-3). We can compensate for this by increasing the air flow, which increases the heat-transfer coefficient, but this drives up operating costs. Generally, DCHX provides closer temperatures approaches than the finned-tube heat exchanger before the costs increase rapidly. [The curves for the DCHX for a given  $Ua$  increase for low outlet air temperature because the volumetric heat-transfer coefficient has been artificially fixed, and the only way to reduce outlet temperature is to increase air flow, which drives up the cost. For  $Ua = 2000 \text{ W/m}^3 \text{ }^\circ\text{C}$  this effect is generally not seen for the temperature approaches presented (less than  $30^\circ\text{C}$ ).]

Calculations at the higher operating pressure (5 atm) were for  $5 \text{ MW}_{\text{th}}$  or  $2 \text{ MW}_{\text{th}}$  heat duty, while those for 1 atm pressure were for  $1 \text{ MW}_{\text{th}}$ . These generally resulted in maximum-sized packed columns ( $5 \times 5 \text{ m}$ ) at the close approaches. Larger columns can be built, but since the cost data were restricted to 5-m-diameter columns, we restricted the calculations to this diameter for consistency. Also, the finned-tube heat exchanger tended to reach maximum size ( $900 \text{ m}^2$ ) before the DCHX. This is seen in the curves for the finned-tube heat exchanger, which show the change of slope (Figure 4-5, for example). These slope changes occur because multiple heat exchangers are used to meet the heat duty. Therefore, one major conclusion we can make is that DCHX provides substantially more heat-transfer capacity for a given size of equipment.

The cost advantage of DCHX relative to finned-tube heat exchangers is not a strong function of approach temperature (difference between salt inlet and air outlet temperatures) except for small temperature approaches where the cost of the finned-tube heat exchanger increases more rapidly. Table 4-3 gives the cost ratios from all six graphs at a  $10^\circ\text{C}$  approach. We used the DCHX curve for  $Ua = 3000 \text{ W/m}^3 \text{ }^\circ\text{C}$  in each case.

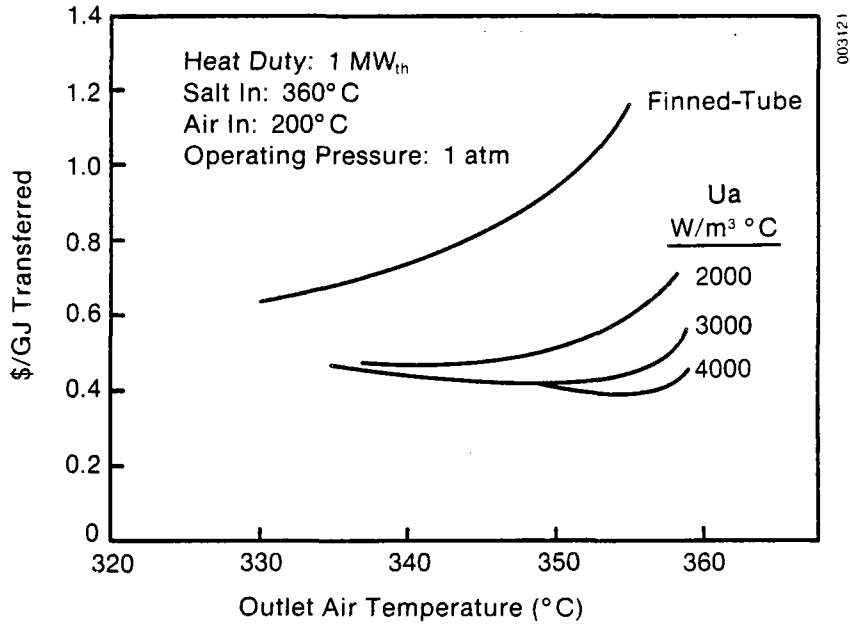


Figure 4-4. Cost Comparison for 360°C, 1 atm, 1 MW<sub>th</sub>

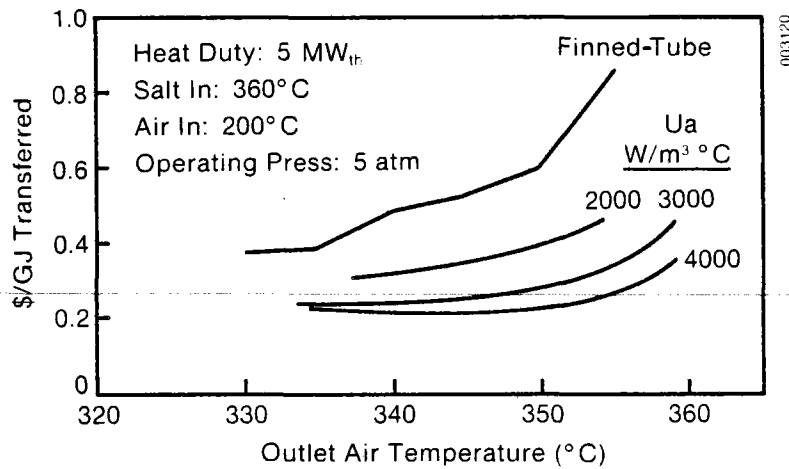


Figure 4-5. Cost Comparison for 360°C, 5 atm, 5 MW<sub>th</sub>

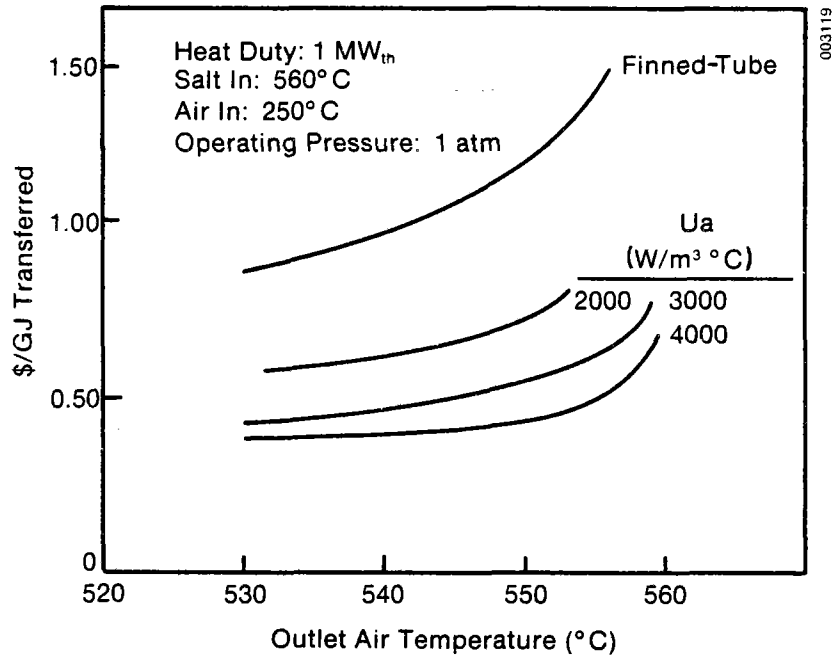


Figure 4-6. Cost Comparison for 560°C, 1 atm, 1 MW<sub>th</sub>

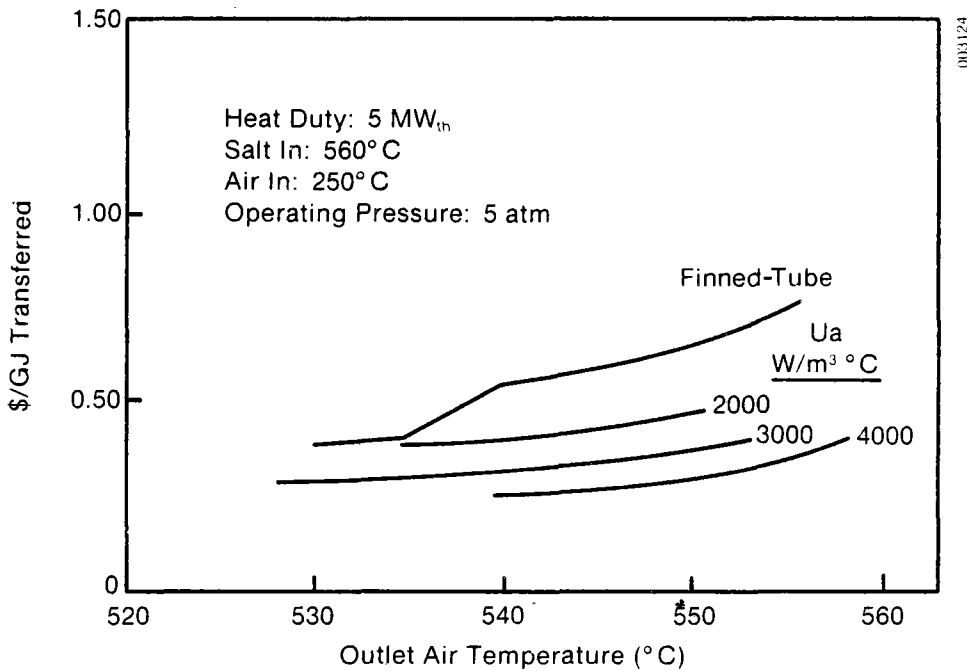


Figure 4-7. Cost Comparison for 560°C, 5 atm, 5 MW<sub>th</sub>

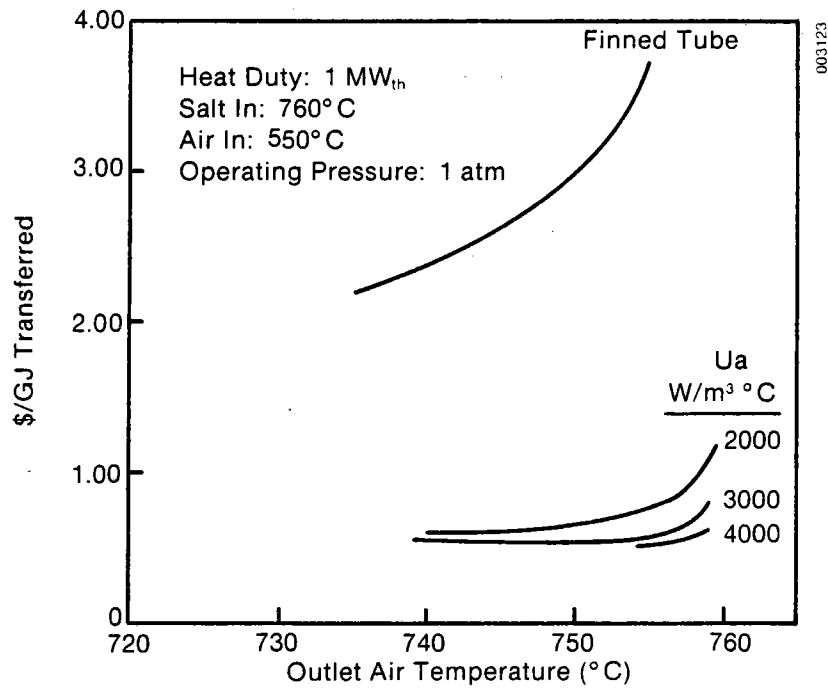


Figure 4-8. Cost Comparison for 760°C, 1 atm, 1 MW<sub>th</sub>

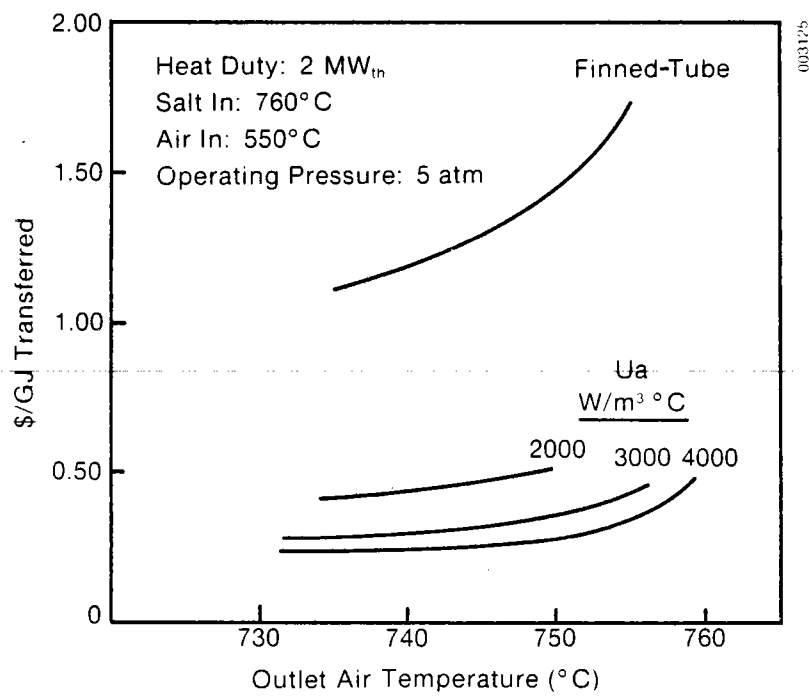


Figure 4-9. Cost Comparison for 760°C, 5 atm, 2 MW<sub>th</sub>

**Table 4-3. Cost Ratios of Transferring Heat via DCHX Relative to Finned-Tube Heat Exchanger**

Temperature (°C)	Operating Pressure	
	(1 atm)	(5 atm)
360	0.44	0.46
560	0.46	0.57
760	0.18	0.26

There appears to be no great decrease in this ratio in going from 360° to 560°C. This is because the cost of construction materials increased substantially for both types of heat exchangers. Using an internally insulated, carbon steel column with stainless steel Pall rings for 560°C operation significantly improves the cost ratio. (Since this represents a larger technical risk than the externally insulated, stainless steel column, it is not a fair comparison to make with commercially available, stainless steel, finned-tube heat exchangers.)

The large reduction in relative cost in going from 560°C to 760°C occurs because the DCHX does not need high alloy steels, while the finned-tube exchanger does require such materials. Even though the high-purity alumina packing is more costly than stainless steel packing, using a carbon steel column provides a very large cost advantage over the Incoloy finned-tube heat exchanger.



## SECTION 5.0

## CONCLUSIONS AND FUTURE RESEARCH

We measured volumetric heat-transfer coefficients in the range of 1800-3500 W/m<sup>3</sup> °C in a 6-in.-diameter column with a 3-ft bed of 0.5-in. metal Raschig rings and 0.6-in. metal Pall rings. The heat-transfer coefficient depends on air flow rate but not on salt flow rate. Heat-transfer coefficients based on mass-transfer data show dependence on both air flow and salt flow. Thus, the mechanisms controlling heat transfer appear to differ from those controlling mass transfer.

The measured heat-transfer coefficients are large enough so one can say with confidence that direct-contact heat exchangers are more cost-effective than conventional finned-tube heat exchangers. At low- to mid-temperatures (360°-560°C), the cost (capital and operating) ratio should be about one-half, while at high temperatures (600°-800°C), where high alloy steels are required in the finned-tube heat exchanger, the cost ratio is about one-fifth. The cost advantage occurs because of the high rates of heat transfer and the ability to use materials other than high alloy steels to contain the salt in the DCHX.

Future research should be directed toward experimentally determining the effect of packing size and type, since in lieu of such data one must project this effect based on mass-transfer data. Since we showed that the heat- and mass-transfer mechanisms are different, this analogy is not a satisfactory approach. At high temperatures, radiation heat transfer will become important. Thus, high-temperature testing, perhaps with internally insulated columns, will be necessary.

To ultimately produce heat-transfer correlations valid over a wide range of operating conditions that will aid designers, it is necessary to understand the mechanisms of heat transfer. A study on separating the effects of radiation, fin-effect, packing wetting, etc., will be helpful.

Any high-temperature (>600°C) experiments on heat transfer must be delayed until materials research has identified compatible heat-transfer salts and containment materials.

**SERIO** 

## SECTION 6.0

## REFERENCES

- Dubberly, L. J., J. E. Gormely, J. A. Kochmann, W. R. Lang, and A. W. McKenzie, 1981(Dec.), Cost and Performance of Thermal Storage Concepts in Solar Thermal Systems, SERI/TR-XP-0-9001-1-B, Golden, CO: Solar Energy Research Institute.
- Fair, J. R., 1972(June), "Designing Direct Contact Coolers/Condensers," Chemical Engineering, pp. 91-100.
- Kays, W. M. and A. L. London, 1964, Compact Heat Exchangers, New York: McGraw Hill.
- Kreith, F., 1976, Principles of Heat Transfer, New York: Harper and Row.
- Martin Marietta Aerospace, 1979(Dec.), Internally Insulated Thermal Storage System Development Program, MCR-79-1369, Denver, CO: Martin Marietta Aerospace.
- Norton Chemical Company, 1977, "Design Information for Packed Towers," Bulletin DC-11, Akron, OH: Norton Chemical Company.
- Peters, M. and K. Timmerhaus, 1980, Plant Design and Economics for Chemical Engineers, New York: McGraw Hill.
- Tortorelli, P. F. and J. H. DeVan, 1982(Dec.), Thermal Convection Loop Study of the Corrosion of Fe-Ni-Cr Alloys by Molten  $\text{NaNO}_3\text{-KNO}_3$ , ORNL/TM-8298, Oak Ridge, TN: Oak Ridge National Laboratory.

**SERI** 

**APPENDIX A**  
**PROPERTY VALUES**

**A.1 VALUES**

We took the constant values for specific heat density and thermal conductivity of the salt from data provided by Park Chemical Company (1983). Constant values of the diffusion coefficient and viscosity and surface tension as a function of temperature were taken from NBS (1981). The values or functions are

$$C = 1553 \text{ J/kg K}$$

$$\rho = 1820 \text{ kg/m}^3$$

$$k = 0.573 \text{ W/m K}$$

$$D = 2.91 \times 10^{-9} \text{ m}^2/\text{s}$$

$$\mu = 90.811 - 0.3517T + (4.665 \times 10^{-4})T^2 - (2.086 \times 10^{-7})T^3 \text{ (cp)}$$

$$\sigma = 155.678 - 0.0627T - (2.315 \times 10^{-7})MT^2 + (5.9877 \times 10^{-7})M^2T \text{ (dyne/cm)}$$

$M = \text{mol \% KNO}_3$

The temperature used in the equations for viscosity and surface tension is the average of the salt inlet and outlet temperatures.

We evaluated air properties at the average of the air inlet and outlet temperatures by the following equations derived from tabular data in Kreith (1976).

$$\rho = 350.8 P/T \text{ (atm, K, kg/m}^3\text{)}$$

$$\mu = (3.5158 \times 10^{-6}) + (4.8240 \times 10^{-8})T - (9.2908 \times 10^{-12})T^2 \text{ (kg/ms)}$$

$$k = (2.719 \times 10^{-3}) + (7.8017 \times 10^{-5})T - (1.1598 \times 10^{-8})T^2 \text{ (W/m K)}$$

$$C_p = 997.9 + 0.143T + (1.10 \times 10^{-4})T^2 - (6.776 \times 10^{-8})T^3 \text{ (J/kg K)}$$

We derived the diffusion coefficient following the procedure in Sherwood, Pigford, and Wilke (1975).

$$D = \frac{(3.555 \times 10^{-5})T^{1.5}}{0.00285\left(\frac{T}{78.6}\right)^2 - 0.06063\left(\frac{T}{78.6}\right) + 1.0739}$$

In the above equations for air properties, we used the average of the inlet and outlet temperatures. All temperatures are in kelvin.

**A.2 REFERENCES**

National Bureau of Standards, 1981, Physical Properties Data Compilations Relevant to Energy Storage, Vol. II: Molten Salts Data on Single and Multi-Component Salt Systems, NSRDS-NBS 61, Washington, DC: NBS.

Park Chemical Company, 1983, Technical Bulletin J-9, Detroit, MI: Park Chemical Co.

Sherwood, T. K., R. L. Pigford, and C. R. Wilke, 1975, Mass Transfer, New York: McGraw Hill.

**APPENDIX B**  
**COSTING METHODOLOGY FOR SERI's SOLAR ENERGY**  
**STORAGE PROGRAM**

Werner Luft

July 1982

## COSTING METHODOLOGY FOR SERI's SOLAR ENERGY STORAGE PROGRAM

In order to ensure comparable cost projections, a consistent methodology and constant financial and economic parameters should be used both by SERI in-house researchers as well as by subcontractors.

The methodology adapted is the one developed by the Jet Propulsion Laboratory [1].

The basic approach of the methodology is to devise an estimate of the costs incurred by the owner/operator of the system as a result of purchasing, installing, and operating the solar energy system under consideration. These costs, aggregated over the system lifetime and converted to an annual basis, are divided by the expected yearly system output. The result is an estimate of the levelized annual cost per unit of output. This levelized cost is the price that must be charged per unit of output so that the resultant revenues would exactly recover the full cost of the system over its expected life. If the levelized annual cost per unit is less than the levelized cost of the same output provided by other means, the system is cost-effective.

The nomenclature and symbols used in this document are explained in Table 1.

The basic equation for the levelized cost is

$$\text{LOC} = \text{AC}/O \quad (1)$$

The levelized annual system cost in  $Y_b$  dollars is computed from the capital expenditures and their timing, as well as the operating and maintenance cost stream. Note that replacement item capital costs are treated as capital expenditures.

The levelized annual system cost is given by:<sup>a</sup>

$$\text{AC} = (1 + g)^{-d} [\text{FCR} \cdot \text{CI}_{\text{pv}} + \text{CRF}_{\text{K,N}} (\text{O\&M}_{\text{pv}} + \text{FL}_{\text{pv}})] \quad (2)$$

The annualized fixed charge rate (FCR) is the factor by which  $\text{CI}_{\text{pv}}$  must be multiplied to obtain the contribution of capital investment to the levelized annual system cost.

The capital recovery factor (CRF) represents the uniform annual amount (payment) that must be made to fully amortize the capital investment (loan) over  $N$  years at the interest rate of  $K$ .

$$\text{FCR}^* = \frac{1}{1 - T} \left( \text{CRF}_{\text{K,N}} - \frac{T}{N} \right) + b \quad (3)$$

<sup>a</sup>Presents value refers to the first year of commercial operation,  $Y_{\text{co}}$ .

\*Disregarding investment tax credit. With investment tax credit FCR is given in Equation (4).



Table 1. Nomenclature

Symbol	Description
a	Investment Tax Credit fraction
AC	Levelized annual system cost in $Y_b$ dollars
ACRS	Accelerated cost recovery system
b	Annual insurance and "other tax" fraction
CI	Capital expenditures
CRF	Capital recovery factor
d	Time difference
DPF	Depreciation factor for Sum-of-the-Years-Digits depreciation
FCR	Annualized fixed charge rate
FL	Fuel Cost
g	Annual rate of general inflation
$g_c$	Annual escalation rate for capital costs
$g_f$	Annual escalation rate for fuel costs
$g_o$	Annual escalation rate for Operation and Maintenance Costs
j	Time difference
K	Cost of capital (Rate of return on Capital, Discount rate)
LOC	Levelized annual cost per unit of output
n	Accounting lifetime (depreciation life or tax life)
N	System operating lifetime
O	Annual System output as measured in MJ
O&M	Operating and Maintenance Costs
p	Time difference
SDF	Depreciation Factor for statutory accelerated depreciation
T	Effective Corporate Income Tax Rate
V	Levelized annual value of system output
$V_o$	Value of system output in year $Y_{co}$ expressed in $Y_b$ dollars
$Y_b$	Base year for constant dollars
$Y_{co}$	First year of commercial operation
$Y_p$	Price year for cost information
$Y_t$	Year t
<hr/>	
Subscript	
<hr/>	
n	Accounting lifetime
N	System operating lifetime
o	Cost year $Y_{co}$ expressed in $Y_b$ dollars
pv	Present value, (year $Y_{co}$ value)
t	Time

$$FCR = \frac{CRF_{K,N}}{1-T} [1 - (T \cdot DPF_{K,n})^{-a}] + b \quad (4)$$

$$CRF_{K,N} = K/[1 - (1 + K)^{-N}] \quad (5)$$

The present value of the capital expenditures and of the operating and maintenance costs are computed using typical discounting formulas. In calculating the present value of the operating and maintenance costs it is assumed that these costs are uniform streams over the system lifetime.

$$CI_{pv} = (1 + g_c)^P \sum_t CI_t \frac{1 + g_c^j}{1 + K} \quad (6)$$

$$O\&M_{pv} = (1 + g_o)^P \cdot O\&M_o \frac{1 + g_o}{K - g_o} \left[ 1 - \frac{1 + g_o^N}{1 + K} \right] \quad \text{if } K \neq g_o \quad (7)$$

$$(1 + g_o)^P \cdot O\&M_o \cdot N \quad \text{if } K = g_o$$

$$p = Y_{co} - Y_p \quad (8)$$

$$j = Y_t - Y_{co} + 1 \quad (9)$$

$$d = Y_{co} - Y_b \quad (10)$$

Note that  $CI_{pv}$  and  $O\&M_{pv}$  are in year  $Y_{co}$  dollars. Adjustment to  $Y_b$  dollars is made when calculating AC.

$O\&M_o$  is the cost in year  $Y_{co}$  expressed in  $Y_p$  dollars.  $CI_t$  is the capital investment during year  $Y_t$  expressed in  $Y_p$  dollars.

For non-uniform operating and maintenance costs,  $O\&M_{pv}$  is calculated from:

$$O\&M_{pv} = (1 + g_o)^P \cdot \sum_{j=1}^N O\&M_t \frac{1 + g_o^j}{1 + k} \quad (11)$$

Based upon the present value estimates for the capital expenditures, the recurrent costs, and operating and maintenance costs, the annual levelized system cost is calculated. This annualized system cost is equal to a cost stream of equal annual payments that has a present value equal to that of all the system costs (i.e., capital expenditures, operating, maintenance, and fuel costs).

For storage subsystem analysis, where several options for storage are considered, and where no annual system output can be associated with the subsystem (but only a storage capacity), present worth for capital costs, operation and maintenance costs, and fuel costs (gas, oil or electricity) may be used in the trade-off.

For accounting purposes, the capital investment must be depreciated over a number of years. For the equipment under consideration the accounting lifetime is 15 years. According to the tax law of 1981, the accelerated cost recovery system (ACRS) may be used. For investments after 1985, the depreciation factor for statutory accelerated depreciation is:

$$SDF_{K,N} = \frac{1}{n(1+K)} \left[ 1 + \frac{2}{CRF_{K,(n-1)}} - \frac{2(1+K)}{nK^2} \left\{ 1 - \frac{1+nK}{(1+K)^n} \right\} \right] \quad (12)$$

The accelerated depreciation schedule for a public utility (15-year accounting life) is shown in Table 2.

**Annual Output Value**

The basic equation for the levelized cost requires an estimate of the system output.

The output value should also be expressed as a levelized annual value using the same discount and inflation factors given in Table 3. To calculate the levelized value of the output the following expression is used.

$$V = V_0 \frac{1+g}{K-g} \left[ 1 - \frac{1+g}{1+K} \right]^N \cdot CRF_{K,N} \quad (13)$$

**Table 2. Accelerated Depreciation Schedule for Public Utility Placed into Service After 31 December 1985 (in percent)**

If the year since installation is:	Applicable percentage
0	7
1	12
2	12
3	11
4	10
5	9
6	8
7	7
8	6
9	5
10	4
11	3
12	3
13	2
14	1

**Table 3. Financial Parameters for Preliminary Economic Analyses**

Symbol	Description	Value
N	System Operating Lifetime	30 years
n	Accounting Lifetime	15 years
K	Cost of Capital (Rate of Return on Capital, discount rate)	0.10 <sup>a)</sup>
CRF <sub>K,N</sub>	Capital Recovery Factor (10%, 30 years)	0.10608
g	Rate of General Inflation	0.06
g <sub>c</sub>	Escalation Rate for Capital Costs	0.06
g <sub>o</sub>	Escalation Rate for Operating and Maintenance Costs	0.06
g <sub>f</sub>	Escalation Rate for Fuel Costs	0.08
Y <sub>b</sub>	Base Year for Constant Dollars	1981
Y <sub>co</sub>	First Year of Commercial Operation	1990
Y <sub>p</sub>	Price Year for Cost Information	1981
	Raw Land Cost	\$1.25/m <sup>2</sup>
	1990 Costs in 1981 dollars for:	
	Natural Gas	\$6.30/GJ
	Residual Oil (No. 6)	\$7.49/GJ
	Distillate Oil	\$8.91/GJ
	Liquid Gas	\$6.83/GJ
	Coal	\$2.28/GJ
	Electricity	\$12.89/GJ
FCR	Annualized Fixed Charge Rate	0.19216
b	Annual Insurance + "Other Tax" Fraction	0.02
a	Investment Tax Credit fraction	0.10
T	Effective Corporate Income Tax Rate	0.50

a) Typical for utility applications. Cost for industrial applications may be higher.

For the given values of the discount factor and the inflation rate, the above expression for the levelized annual output value reduces to:

$$V = 1.88584 V_0$$

The financial parameters to be used are given in Table 3.

### Capital Investment Estimation

Cost estimation for capital equipment shall use the methodology and factors given in References 2 and 3.

### Cost Comparisons

For energy storage cost estimates, the capital investment in equation (6) can be approximated by:

$$CI_t = F_1 [F_2 (A) + F_3 (B)] \quad (14)$$

where

- A = Energy and power related capital costs of system
- B = Storage medium cost.
- F<sub>1</sub> = Non-direct costs factors
- F<sub>2</sub> = Installation cost factor for A
- F<sub>3</sub> = Installation cost factor for B

The magnitude of the factors F<sub>1</sub>, F<sub>2</sub>, and F<sub>3</sub> vary widely for various groups that have made cost estimates. Table 4 shows the values for these factors.

For SERI work, the factor per Reference 3 shall be used. Derivations from these factors must be justified.

Table 4. F-Factors

Source	F <sub>1</sub>	F <sub>2</sub> <sup>b</sup>	F <sub>3</sub> <sup>c</sup>	(F <sub>1</sub> ) x (F <sub>2</sub> )
Ref. 3	1.95	1.80	1.0	3.51
Industry Practice <sup>a</sup>				
Maximum	2.5	2.0	2.0	5.0
Minimum	--	--	1.0	3.0
JPL	1.2	1.0	1.0	1.2
SNLL	1.155	--	--	TBD
SNLA	1.25	--	--	TBD
Solar Thermal Cost Goals Committee	1.25	TBD	TBD	TBD
Copeland (6/81 \$ 2/82)	1.44	1.8	1.0	2.59

<sup>a</sup>According to Stearns-Roger Services, Inc.

<sup>b</sup>The installation cost factor is based on the primary equipment cost. It gives an estimate for the labor cost to install the equipment.

<sup>c</sup>F<sub>3</sub> is the labor cost factor to install the storage medium.

## REFERENCES

1. Doane, J. W.; O'Toole, R. P.; Chamberlain, R. G.; Bos, P. B.; Maycock, P. D. The Cost of Energy from Utility-Owned Solar Electric Systems--A Required Revenue Methodology for ERDA/EPRI Evaluations. ERDA/JPL-1012-76-3. Pasadena, CA: Jet Propulsion Laboratory; June 1976.
2. Plant Design and Economics for Chemical Engineers. Max Peters and Ulaus D. Timmerhaus. Publ. McGraw-Hill Book Company, 1980.
3. Cost and Performance of Thermal Storage Concepts in Solar Thermal Systems, Final Report Phases 1 and 2, SERI/TR-XP-0-9001-1-A and -B. November and December 1981. Prepared by Stearns-Roger Services Inc., Denver Colo. Available from NTIS.

<b>Document Control Page</b>	1. SERI Report No. SERI/TR-252-2015	2. NTIS Accession No.	3. Recipient's Accession No.
4. Title and Subtitle  Air/Molten Salt Direct-Contact Heat Transfer Experiment and Economic Analysis		5. Publication Date November 1983	
7. Author(s) Mark Bohn		8. Performing Organization Rept. No.	
9. Performing Organization Name and Address Solar Energy Research Institute 1617 Cole Boulevard Golden, Colorado 80401		10. Project/Task/Work Unit No. 1375.00	
		11. Contract (C) or Grant (G) No. (C)  (G)	
12. Sponsoring Organization Name and Address		13. Type of Report & Period Covered Technical Report	
15. Supplementary Notes		14.	
16. Abstract (Limit: 200 words) Direct-contact heat-transfer coefficients have been measured in a pilot-scale packed column heat exchanger for molten salt/air duty. Two types of commercial tower packings were tested: metal Raschig rings and initial Pall rings. Volumetric heat-transfer coefficients appeared to depend upon air flow but not on salt flow rate and were measured.			
An economic analysis was used to compare the cost-effectiveness of direct-contact heat exchange with finned-tube heat exchanger in this application. Incorporating the measured volumetric heat-transfer coefficients, a direct-contact system appeared to be from two to five times as cost-effective as a finned-tube heat exchanger, depending upon operating temperature. The large cost advantage occurs for higher operating temperatures (2700°C), where high rates of heat transfer and flexibility in materials choice give the cost advantage to the direct-contact heat exchanger.			
17. Document Analysis			
a. Descriptors Air ; Column packing ; Direct contact heat exchangers ; Economic analysis ; Flow rate ; Heat exchangers ; Heat transfer ; Mass transfer ; Molten salts			
b. Identifiers/Open-Ended Terms			
c. UC Categories 59c			
18. Availability Statement National Technical Information Service U.S. Department of Commerce 5285 Port Royal Road Springfield, Virginia 22161		19. No. of Pages 63	
		20. Price A04	